# A STUDY OF FATIGUE CRACK INITIATION AND SHORT CRACK GROWTH IN A MONEL ALLOY

By

GEORGE OWEN WILSON

Bachelor of Science

in Mechanical Engineering

Oklahoma State University

Stillwater, Oklahoma

1987

Submitted to the Faculty of the
Graduate College of the
Oklahoma State University
in partial fulfillment of
the requirements for
the Degree of
MASTER OF SCIENCE
July, 1989

A STUDY OF FATIGUE CRACK INITIATION
AND SHORT CRACK GROWTH
IN A MONEL ALLOY

Thesis Approved:

C. E. Price
Thesis Advisor

J. K. Good

R. I. Stephens

Norman N. Durham
Dean of the Graduate College

## ACKNOWLEDGEMENTS

I wish to express sincere appreciation to Dr. C. E. Price for his instruction, encouragement, and advice throughout this undertaking. Thanks also are extended to Dr. Good and Dr. Lowery for serving as committee members.

The School of Mechanical and Aerospace Engineering at Oklahoma State University provided a needed teaching assistantship which allowed me to pursue this degree. Also provided were the necessary materials and equipment.

Thanks are extended to James and Mary Wilson, and also Louis and Mary Jo LaDuron whose encouragement and support were invaluable. Thanks also to my wife, Linette, and my children who supported and endured my continued education.

TABLE OF CONTENTS


| Chapter | | Page |
|---|---|---|
| I. | INTRODUCTION | 1 |
| II. | REVIEW OF THE LITERATURE | 5 |
| | Fatigue | 5 |
| | Embrittlement | 14 |
| | Liquid Metal Embrittlement | 14 |
| | Sulfur Embrittlement | 17 |
| | Hydrogen Embrittlement | 18 |
| | Stress Corrosion Cracking | 19 |
| | Comparison with Other Nickel Alloys | 19 |
| III. | EXPERIMENTAL PROCEDURES | 21 |
| | Material | 21 |
| | Specimen Geometry | 21 |
| | Specimen Preparation | 21 |
| | Fatigue Sequence | 24 |
| IV. | EXPERIMENTAL RESULTS | 27 |
| | Slip Behavior | 27 |
| | Plastic Zone | 31 |
| | Crack Initiation | 31 |
| | Crack Growth | 34 |
| | Fatigue Hardening | 40 |
| | Cracking Mode | 50 |
| V. | DISCUSSION | 52 |
| VI. | CONCLUSIONS | 59 |
| A | SELECTED BIBLIOGRAPHY | 61 |

# LIST OF TABLES


| Table | | Page |
|---|---|---|
| I. | Chemical Composition . . . . . | 23 |
| II. | Inspection Interval . . . . . | 25 |

LIST OF FIGURES


| Figure | | Page |
|---|---|---|
| 1. | Development of an Extrusion-Intrusion Pair | 7 |
| 2. | Plastic-Blunting Mechanism | 9 |
| 3. | Intense Shear Bands | 10 |
| 4. | Stage I and Stage II Crack Growth | 11 |
| 5. | Effect of Nickel Content on Required Phosphorus | 16 |
| 6. | Crack Propagation in Reversed Bending | 29 |
| 7. | Crack Propagation in Reversed Bending with Cold Work | 30 |
| 8. | Surface Rumpling Under Axial Fatigue | 32 |
| 9. | Plastic Deformation at Notch | 33 |
| 10. | Crack Branching | 35 |
| 11. | Crack Length vs Number of Cycles | 37 |
| 12. | Crack Growth Rate vs Crack Length | 38 |
| 13. | Crack Growth Rate vs Stress Intensity Range | 39 |
| 14. | Cracking Under Axial Loading | 41 |
| 15. | Cracking Under Reversed Bending | 42 |
| 16. | Crack Length vs Cycles for Reversed Bending, Life Greater than 2.5 Million Cycles | 43 |
| 17. | Crack Length vs Cycles for Reversed Bending, Life of About 1 Million Cycles | 44 |

Figure Page

18. Crack Length vs Cycles for Reversed Bending, Life Equal to 73,000 Cycles . . . . . 45

19. Axial Hardness Profile for Coarse Grains . . . . . 47

20. Axial Hardness Profile for Fine Grains . . . . . 48

21. Axial Hardness Profile for an Unbroken Specimen . . . . . 49

22. Percentage Intergranular Fracture vs Grain Size . . . . . 51

23. Fine Grain Axial Fatigue Fracture Surface . . . . . 57

## LIST OF SYMBOLS

| | |
|---|---|
| a | crack length |
| da | change in crack length |
| dK | range of stress intensity |
| dN | change in number of cycles |
| EAC | environmental assisted cracking |
| HE | hydrogen embrittlement |
| HV | Vickers hardness |
| IG | intergranular |
| dK | stress intensity range |
| LEFM | linear elastic fracture mechanics |
| LME | liquid metal embrittlement |
| MVC | microvoid coalescence |
| OPA | optimum aged |
| OVA | over aged |
| PSB | persistent slip band |
| SC | microstructurally short cracks |
| SCC | stress corrosion cracking |
| SFE | stacking fault energy |
| SHT | solution heat treated |
| SSRT | slow strain rate test |
| TG | transgranular |

# CHAPTER I

## INTRODUCTION

When a designer has a corrosion problem he chooses a material which is resistant to the environment of interest. A common choice for reducing or mildly oxidizing environments are the nickel-copper alloys of the Monel family (1,12). These alloys are economical, easily joined, and have good hot and cold formability. Additionally, the strongest of the nickel-copper alloys, Monel K500 (N05500), can be age hardened to a yield strength of about 750 MPa. However, over the years, a number of service failures have occurred unexpectedly due to environmental assisted cracking (EAC) which were usually intergranular (IG) in nature. For example (5), some 6 inch long, 3/4 inch diameter Monel bolts were used to fasten externally flanged joints on pipe lines carrying anhydrous hydrogen fluoride at atmospheric temperature. When leaks occurred at the joints the bolts failed in 5 to 15 hours. Cracking was both IG and transgranular (TG) for bolts which had been hot rolled and aged, and completely TG for bolts which were cold drawn and aged.

In another case (5), a 10-foot length of tubing was used as a depth gauge in a storage tank containing 20 to 25

percent hydrofluorosilicic acid at 120 F. After a time the tube split over its entire length. The cracking was entirely IG.

A third example (16) involves cracks which were observed after welding right angle slow bend sections of Monel 400 90 mm outside piping to straight sections of piping of the same alloy. The cracks were in circumferential directions in the weld heat affected zone and were entirely IG in nature. Subsequent investigation revealed the bends had contacted a molten mixture of lead and bismuth during manufacture. The combination of heat and stress provided by the welding process was sufficient to induce IG cracking in the vitiated material.

A final example (7), hardened Monel bolts were used to secure the main, load-bearing, riser clamps on a platform in the UK North Sea. The bolts failed due to hydrogen charging caused by the cathodic protection system. Cracking was highly branched and completely IG.

As illustrated by the examples, these alloys are susceptible to hydrogen embrittlement (HE), liquid metal embrittlement (LME), and stress corrosion cracking (SCC). While any nickel base alloy can experience EAC under appropriate conditions, it is in the nickel-copper alloys that the susceptibility is the greatest, greater than that of the constituent metals nickel and copper (29). There is no obvious answer as to why this should be so; one factor is the apparent ease with which IG cracking occurs.

A particularly invidious situation is fatigue loading in an active environment. In such a case, the fatigue life of Monel alloy may be reduced by several orders of magnitude with a brittle IG fracture occurring (19,29). This, when the fatigue properties of the alloy in air are already mediocre. The reversed bending fatigue limit of the age hardenable alloy, Monel K500 (N05500), is below half of the yield strength and is little more than the limit in the annealed or solution-heat-treated condition (1). Even in air, fatigue cracking is predominately IG (27).

The purpose of the present investigation is to study further this propensity towards IG cracking in air and to determine whether meaningful crack growth relationships can be obtained when IG cracking dominates. Comparisons will be made to two previous studies, the work of Henderson (27) on fatigue cracking in Monel K500, and a report by Ho (11) on crack growth relationships in nickel.

Heat treatment will not be a variable as Henderson (27) showed the cracking behavior of Monel was insensitive to heat treatment. However, a coarse grain size will be used to facilitate observations of the slip behavior and fatigue crack growth inside the grains. Also, IG cracking is usually associated with grain boundary impurities. By growing a coarse grain size at elevated temperature and then quenching, the segregation of impurities at the grain boundaries should be minimized.

Other objectives are to investigate the fatigue

hardening behavior, the role of inclusions, and differences between axial and bending fatigue.

# CHAPTER II

# REVIEW OF THE LITERATURE

## Fatigue

The normal progression of fatigue damage is usually divided into three stages:

1. Crack initiation.
2. Stage I crack growth.
3. Stage II crack growth.

Pre-crack damage accumulation occurs by the movement of dislocations along major slip planes. As dislocations move and stackup they produce a deformed area seen as a slip band. Slip bands often intensify to form structures called persistent slip bands (PSBs). PSB formation is facilitated by easy cross-slip and is therefore most commonly found in high stacking fault energy (SFE) alloys. Aluminum and nickel are examples of high SFE metals. Yellow brass and austenitic stainless steels have a low SFE, <10mJ/m^2 (10). Nickel base alloys typically have a medium SFE as alloying elements tend to lower the SFE (13). This medium SFE would indicate that cross-slip would be relatively difficult but could occur.

Slip bands tend to form along slip planes aligned with the direction of greatest shear. This occurs at 45 degree

angles from the load axis. These bands intensify and lengthen until they span the grain. Material inside the slip band tends to cyclically soften, allowing cracks to form. Neumann, Fuhlrott, and Vehoff (20) described a process whereby repeated compressive and tensile loading tended to create extrusions and intrusions in the softened material as shown in figure 1. Extrusions and intrusions in the slip band create a crack which then grows across the grain. When the crack tip reaches the grain boundary it either links up with a crack from the neighboring grain, continues growth by cross-slip to a suitably aligned slip plane, or the crack is blunted and ceases to grow. In the third case, alternate cracks grow to continue the damage process.

Stage I crack propagation is simply the process of a major crack forming from the smaller cracks. First a crack forms at a slip band within a grain and then grows to the grain boundary. At the grain boundary, the crack links up with a crack which has developed in the target grain, or induces a crack to grow in the target grain after which crack linkage occurs. In this way the crack propagates along slip planes, usually oriented close to 45 degrees with respect to the load axis.

Stage II crack propagation is defined as crack growth which is roughly perpendicular to the load axis. Laird (14) has described how the alternate loading found in fatigue causes crack growth by a plastic-blunting mechanism. In

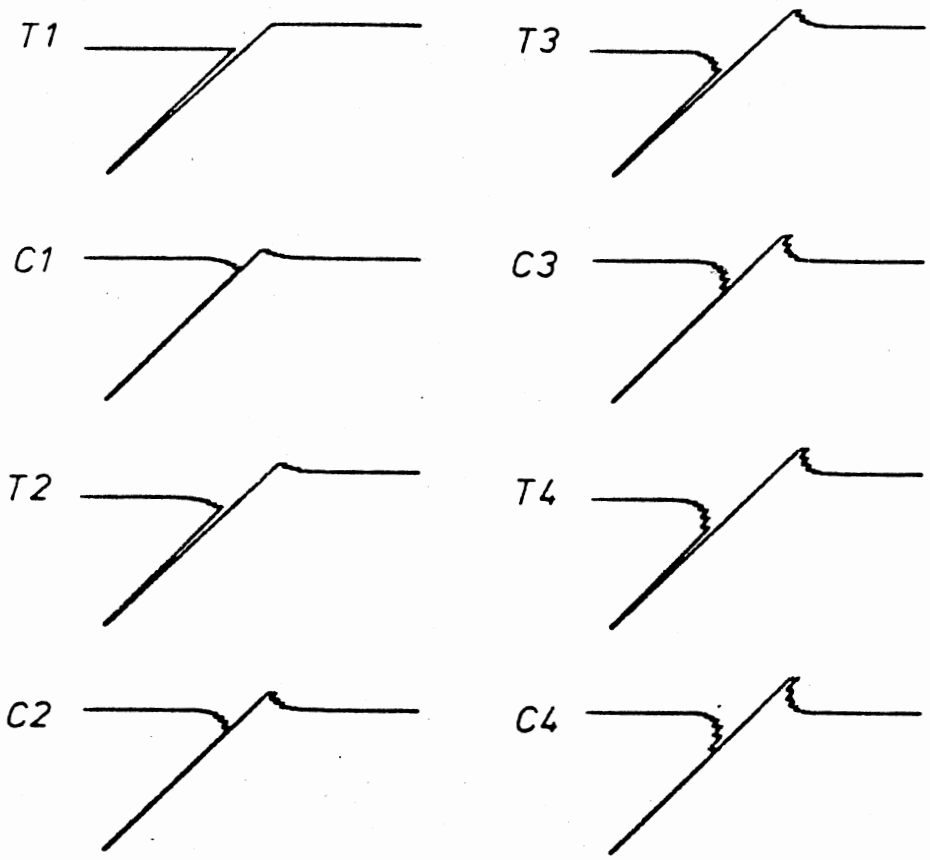


Figure 1. Development of an Extrusion-Intrusion Pair. The profile of the surface is shown after four tension (T) and compression (C) cycles (Neumann et al, Ref 20).

this process, shown in figure 2, a tear forms at the crack tip thus lessening the shear stress and blunting further growth. The compressive cycle changes the blunted end to two small notches. These notches serve to concentrate the stresses during the next cycle to induce further tearing. Evidence of this process is seen as striations on fatigue fracture surfaces.

Neumann (20) demonstrated stage II crack propagation to be a process whereby opposing slip bands, each at 45 degrees from the load axis, alternate in propagating the crack across the material. This was demonstrated by straining an Fe-3Si crystal in a Scanning Electron Microscope. Figure 3 illustrates the position and orientation of intense shear bands which form at the crack tip due to the severe shear stresses which occur at 45 degrees from the load axis.

Thus, the final fracture usually shows two stages to fatigue crack propagation as indicated in figure 4. The first being stage I followed by stage II. Bear in mind that this is not the only order for these to occur. The transition from stage I to stage II is thought to occur due to an increase in the stress at the crack tip. By decreasing the load amplitude, and thereby reducing the stress at the crack tip, Neumann and colleagues (20) have shown stage I growth can be induced after the transition has been made to stage II growth.

Recently interest has focused on the behavior of microstructurally short cracks (SC), usually less than three

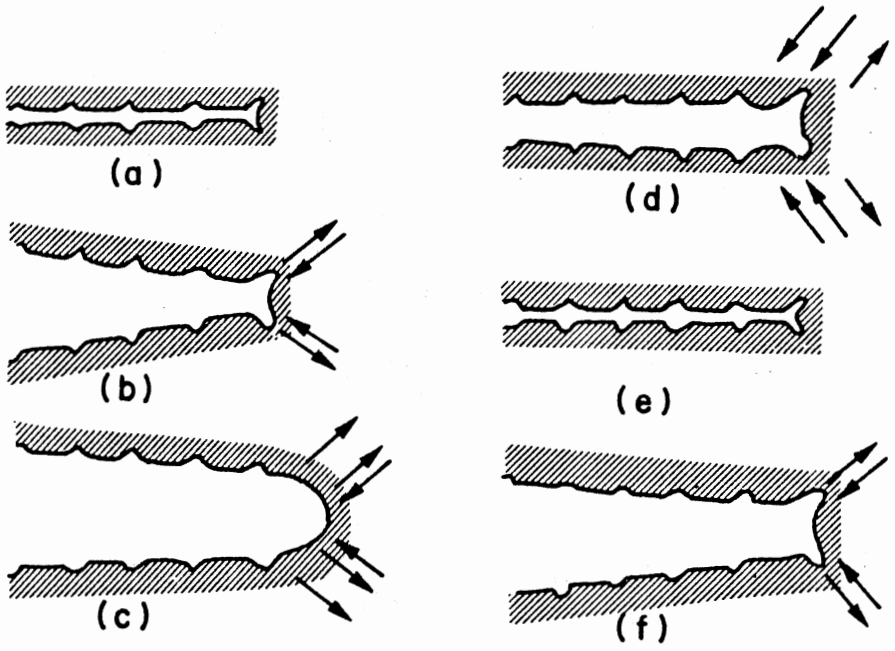


Figure 2. Plastic-Blunting Mechanism: (a) zero load; (b) small tensile load; (c) maximum tensile load; (d) small compressive load; (e) maximum compressive load; (f) small tensile load. Stress axis is vertical (Laird, Ref 14).

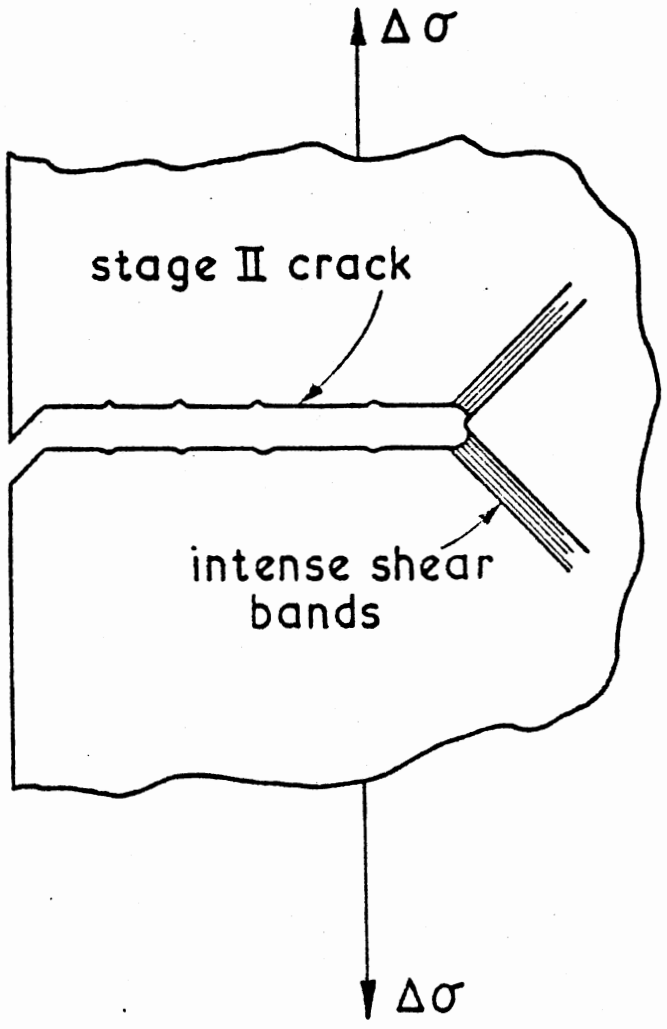


Figure 3. Intense Shear Bands: This illustrates how the maximum shear stresses act during stage II crack propagation.

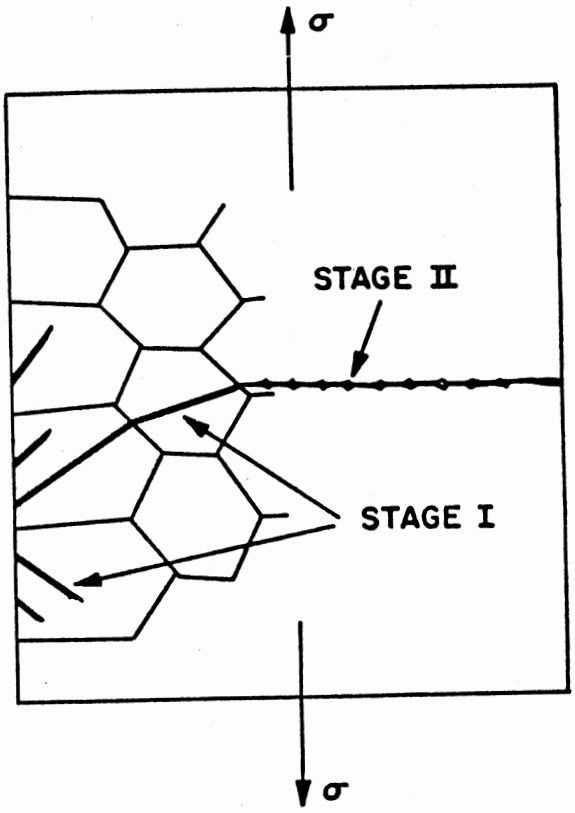


Figure 4. Stage I and Stage II Crack Growth . (Laird Ref 14).

grains in length, as such growth can account for a major portion of the fatigue life. There are a number of models to describe SC growth but a common theme is that linear elastic fracture mechanics does not apply, and microstructural barriers such as grain boundaries and inclusions impede crack growth (18). Note that SC propagation coincides with stage I crack growth, the former being an attempt to expound upon the later.

While most papers on SC growth behavior refer to aluminum alloys, Ho (11) investigated crack initiation and short crack growth in nickel during reversed bending fatigue. He reported TG crack initiation within the first 1% of the life. Initial growth was quick but slowed as the crack approached a grain boundary. After the crack crossed the grain boundary, the rate of propagation was slow and irregular. This slow irregular growth persisted until the crack was about three grains in length (1200-1500 um). Having spent about 3/4 of the life in crack initiation and SC growth, the crack propagation rate then increased and the crack grew in a more regular fashion until failure, with the stress intensity the major criterion.

Once a crack has left the SC growth regime, linear elastic fracture mechanics (LEFM) is applicable and fatigue crack propagation becomes mainly dependant upon the stress intensity at the crack tip. This corresponds to stage II crack growth. Paris (22) postulated that the stress intensity factor, itself a function of stress and crack

length, was the overall controlling factor in stage II fatigue crack growth. He proposed the Paris equation:

$$da/dN = A(dK)^m$$

Where:
- $da/dN$ = crack growth rate
- $dK$ = stress intensity factor range
- $A, m$ = f(material, environment, frequency, temperature, stress ratio)

Hertzberg (10) illustrated how the Paris equation may be used to predict fatigue life once the constants have been determined by experiment.

Frandsen et al (30,31) have reported on the fatigue properties of alloy 500 at ambient temperature in vacuum, oxygen, and hydrogen. Double cantilever beam specimens were used in the peak hardened condition with 25 um grain size. Fracture in vacuum and oxygen was found to be TG and ductile. Price and Good (25) also found TG propagation with crystallographic crack initiation in air.

Price and Henderson (27) investigated the progression of reversed bending with cantilever beam specimens of alloy 500 with a 25um grain size in air. They found about 20 HV of hardening near the final fracture in over-aged (OVA) and solution-heat-treated (SHT) specimens. Hardening was not observed in the optimum-aged (OPA) condition. However, about 80% IG fracture was observed in all conditions. The progression of cracking was IG to TG to TG with striations and final fracture by microvoid coalescence. Inclusions did not appear to play a significant role in crack initiation or subsequent propagation.

While IG cracking has been observed in Monel sans

active environment, such cracking is usually associated with material which has been embrittled by heat treatments or the environment. Such IG crack propagation occurs at a rate of one or more orders of magnitude greater than TG propagation for the same material (19,30,31).

## Embrittlement

The nickel-copper alloys have been shown to be susceptible to embrittlement by several means:

1. Hydrogen environment.
2. Sulfur at the grain boundaries.
3. Liquid metal embrittlement.
4. Stress corrosion cracking.

While the conditions and actions of these environments may differ, there is a common theme to their action. The embrittling species usually acts at the grain boundary to weaken local bonds and thus cause preferential IG fracture.

### Liquid Metal Embrittlement

The Monel alloys have been found to be embrittled by mercury, lead, and lithium (1,16,21,24). Price and Good (25,26) found Monel to be more embrittled by mercury than other nickel alloys both in slow strain rate testing and in fatigue. Fracture under both type of loading was brittle and intergranular. Price and Fredell (24) found embrittlement in mercury to be maximum with a 250 um grain size. Interestingly, Costas (6) has shown that additions of

phosphorus can reduce the embrittling effect of mercury on nickel alloys.

Costas (6) found that phosphorus can reduce mercury embrittlement in alloys which contain nickel. Additionally, figure 6 shows that the amount of phosphorus needed for a given degree of protection depends upon the amount of nickel in the alloy. The mode of action of the phosphorus is not known, but Funkenbusch, Heldt, and Stein (9) reasoned that phosphorus may improve the atomic packing at grain boundaries and free surfaces, thereby decreasing the ability of the mercury to find ingress.

Parikh (21) used flat specimens, wetted on one side, to investigate embrittlement by molten lithium. The wetted fracture stress of annealed Ni-Cu was about 63 MPa for all compositions from 5% to 100% nickel. The fracture surfaces of pure nickel had a mixture of IG and TG with single slip and an absence of cross-slip beneath the lithium, and extensive cross-slip on the unwetted surface.

Additionally, fracture stress was independent of strain hardening due to cold work and showed slight dependence on grain size. Parikh (21) felt this indicated the process of fracture initiation occurs at an early stage of deformation and may not be explained by dislocation pileup. Later analysis of sulfur embrittlement by Messmer and Briant (17) may help to explain the mechanics of LME.

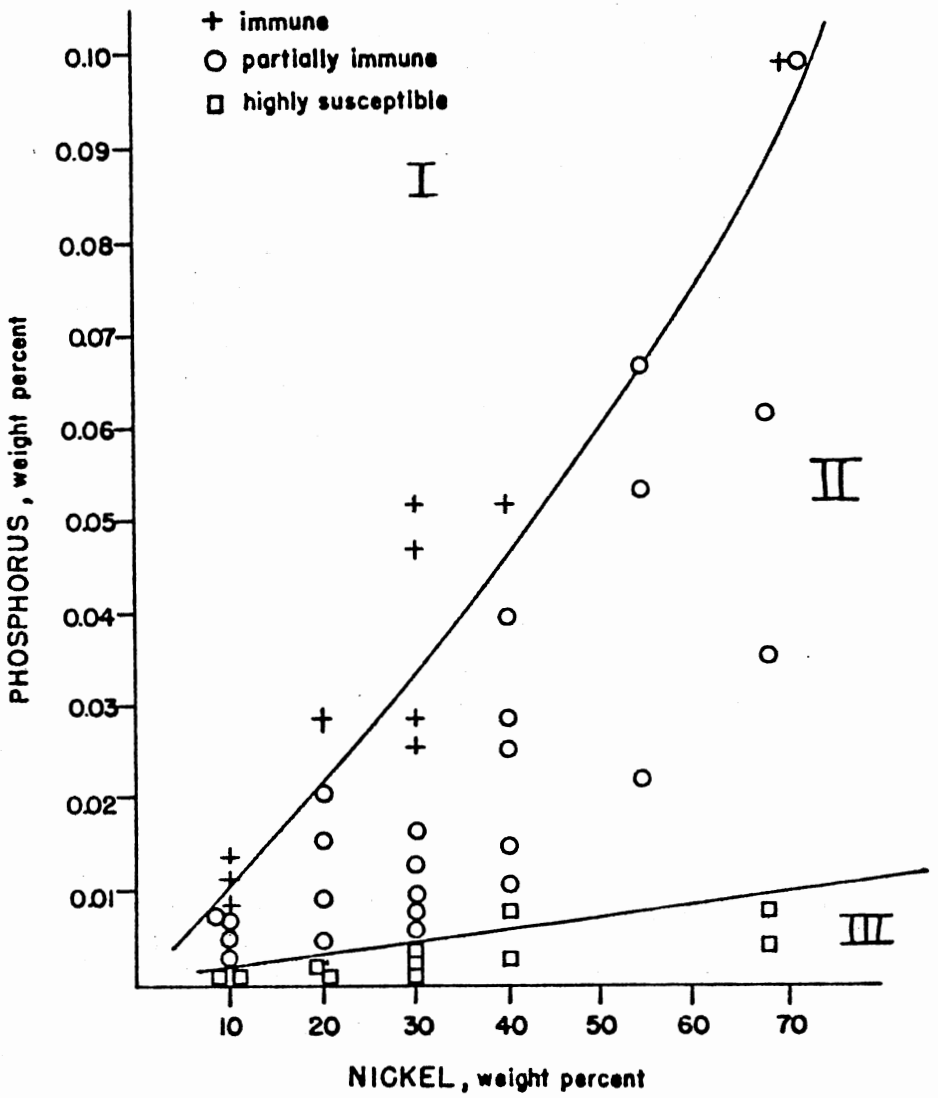


Figure 5. Effect of Nickel Content on Required Phosphorus (Costas Ref 6).

Sulfur Embrittlement

Sulfur is known to embrittle nickel based alloys when it is segregated at the grain boundaries. Such segregation can be avoided by distributing the sulfur with a 900 C anneal followed by a rapid quench (33). Holding the quenched material in the range of 450-850 C will allow the sulfur to diffuse preferentially to the grain boundaries (4). Messner and Briant (17) have proposed a model for embrittlement based upon the chemical bonds which are formed when impurities react with a host alloy.

For a strong embrittler, such as sulfur in nickel, the bonds which form concentrate the charge heavily of the impurity atoms and slightly on the metal atoms (17). This makes the impurity electronegative with respect to the metal and results in a bond which could be described as ionic. A cohesive enhancer, such as boron in nickel, shares the charge more equally and thus results in a bond which is approximately covalent.

Messner and Briant (17) propose that when sulfur bonds with nickel it effectively robs charge from the nickel. This leaves less charge for that nickel atom to use in its metallic bonds. The results is less cohesive force at the grain boundary and thus embrittlement. When boron is present at the grain boundary, the metallic bonds in the nickel are unaffected due to equal sharing of charges in bonding. Additionally, the boron adds its covalent bonds

which effectively strengthen the boundary.

Although Messmer and Briant (17) did not analyse the most common embrittler of all, hydrogen, their model would predict embrittlement by hydrogen quite well.

## Hydrogen Embrittlement

Hydrogen is well known as an embrittler of nickel based alloys (3,7,15,19,24). The mechanisms of hydrogen embrittlement (HE) on the Monel alloys are described by Morris et al (19). Hydrogen has been shown to lower the stacking fault energy of face centered cubic (fcc) materials. This locally prevents cross-slip from relieving the stress concentration created by at the boundary the impingement of slip bands at the grain boundaries, thereby promoting IG fracture.

Price and Fredell (24) found mercury to be a stronger embrittler of Monel 400 than hydrogen in slow strain rate tests (SSRT). Interestingly, embrittlement in hydrogen decreased with increasing grain size. Richards and companions (30,31) reported a fracture mode dependence in hydrogen on mean stress intensity. They found an increase in the mean stress intensity resulted in an increase in the fraction of IG fracture. They reasoned a diffusion dependent mechanism where the speed of dislocations would be proportional to the mean stress intensity.

One last point on HE. Lassila and Birnbaum (15) found that the presence of hydrogen in nickel is not enough to

produce embrittlement. The hydrogen must diffuse to the grain boundary. If such diffusion is not allowed to take place, the material is not embrittled.

Stress Corrosion Cracking

While the Monel alloys resist attack by hydrofluoric acid (HF) in all concentrations, they are susceptible to stress corrosion cracking (SCC) at room temperature by aerated hydrofluoric acid (12). Everhart (8) has shown that HF combined with other oxidizers such as cupric fluoride and cupric chloride will also induce SCC in Monel. Cracking in these environments progressed from IG to TG to failure by microvoid coalescence. Further, lowering the yield stress increases the amount of TG cracking in both SCC and LME.

## Comparison with Other Nickel Alloys

The progression of bending fatigue has been reported for several nickel-based alloys. This will provide a useful base for comparison with the present investigation.

Price (23) found slip in Nickel 200 after the first cycle of reversed bending. The slip markings increased in intensity and cracking occurred at slip bands away from the grain boundaries within the first 1% of the life. Slip was concentrated in wide bands which spanned the grains and were quite uniformly dispersed. Cracking started at the center of the bands, well away from the grain boundaries. Slip on third and fourth slip systems was not unusual while a few

isolated grains remained nearly free of slip. As fatigue progressed, the cracks grew to span the grain. Failure occurred by linkage, partly along grain boundaries, of these cracks to form the final fracture with 10% of the fracture being IG. Fatigue cracking did not initiate until the material had hardened from 95 HV to 140 HV. 20 HV of additional hardening occurred during the crack growth phase.

Price and Henderson (27), in a previous study of alloy 500, found the following progression of damage in reversed bending for a 25 um grain size. Slip, observed after the first 4% of the life of the sample, was first associated with inclusions. As testing proceeded, slip increased and the specimen took a mosaic appearance with slip in some grains while others remained featureless. By 80% of the life, cracked slip bands had linked over 3-4 grains, usually by propagation along grain boundaries. Subsequent propagation was usually along grain boundaries with 80% of the fracture being IG, independent of life or material condition. Also found was about 20 HV of hardening in both the SHT and OVA samples with no hardening when in the OPA condition.

Price and Houghton (28) found slip markings after the first reversal for alloy 625. The slip was planar and multiple slip was common. In contrast with Monel, fracture was entirely TG and spread in a zigzag fashion by slip band cracking on two systems. Hardening did not occur except at high strain levels which then produced short lives.

# CHAPTER III

# EXPERIMENTAL PROCEDURES

## Material

Alloy 500 specimens were cut from the unaffected portion of specimens used in the Henderson (27) study. The chemical composition is reported in table I. Although alloy 500 is usually used in the hardened condition, all specimens were heat treated and quenched to obtain the solution heat treated state. This allowed the growth of large grains and, it is reasoned, extension of the results of this study to alloy 400.

## Specimen Geometry

The specimens were 100 by 12.5 by 1.7 mm thick. Two opposite edge notches were cut 1 mm deep and located 20 mm from the clamped end for the reversed bending specimens. Notches were 2 mm deep and centered on the axial fatigue specimens.

## Specimen Preparation

A low-speed diamond saw was used to cut sharp notches with a minimum of cold work induced at the notch surface. Mineral oil, which was used as a lubricant/coolant by the

diamond saw, was cleaned from the sample by careful washing with laboratory detergent.

The specimens were then ground and polished by the following steps:

1. Manual sanding with wet 240 grit SiC paper.
2. Manual sanding with wet 320 grit SiC paper.
3. Manual sanding with wet 400 grit SiC paper.
4. Manual sanding with wet 600 grit SiC paper.
5. Polishing on a wheel with 5 micron alumina.
6. Polishing on a wheel with 1 micron alumina.

This polishing reduced the severity of oxide formation during the subsequent heating.

Specimens were soaked at 1050 C under vacuum for times ranging from one to eight hours. The soak was followed by a quench in 2% ethanol-water solution as recommended by Huntington (12) to suppress oxide formation. The different times in the furnace created a range of different grain sizes from 25 to 500 micrometers for the specimens.

The specimens were ground and polished as described above to remove the thin layer of oxide which had formed. This was followed by an electrochemical polish to prepare the specimens for microscopic inspection. A solution of 33% nitric acid in methanol was used with 3A/cm^2 for 60 seconds to obtain a good polish. This was followed by a 30 second etch cycle to obtain a slight grain boundary etch.

As each notch would initiate a crack on each side of the specimen, the notches and sides were numbered for easy

TABLE I

CHEMICAL COMPOSITION

| Element | Weight per cent |
|---|---|
| Nickel | 64.36 |
| Copper | 30.46 |
| Carbon | 0.17 |
| Manganese | 0.60 |
| Iron | 0.75 |
| Sulfur | 0.005 |
| Silicon | 0.12 |
| Aluminum | 2.99 |
| Titanium | 0.52 |

reference and identification during the fatigue sequence. When not undergoing fatigue or being examined, the specimens were stored in stoppered test tubes with desiccant.

## Fatigue Sequence

Axial specimens were cycled at 35 Hz in a MTS machine in tension-tension for a life of about 150000 cycles. This seemed to yield the most information without excessive time being spent in running the samples. At appropriate intervals the samples were removed for inspection with a Reichert microscope and possible photography. When cycling was resumed, the loads were gradually increased to the testing level. A minimum load of 120 pounds was selected to ensure the sample would not be cycled in compression. The maximum load, usually 600 pounds, was chosen to obtain a reasonable fatigue life. This corresponded to nominal stresses of 25 MPA and 127 MPa respectively.

Bending specimens were fatigued at 35 Hz in fully reversed pure bending utilizing a Budd VSP-150 fatigue machine. Bending specimens were fatigued on settings ranging from 5 to 10 which corresponded to lives of 50000 to much greater than 2.5 million cycles. Specimens were removed at various intervals for inspection and photography as indicated in Table II.

A few specimens were pulled to yielding in the MTS machine to produce cold work. These were then fatigued either axially or with reversed bending to find the effect

TABLE II

INSPECTION INTERVAL

| Specimen: | One | Two | Three | Four |
|---|---|---|---|---|
| # of Cycles (X 1000) | 0.1 | 0.1 | 0.1 | 0.1 |
| | 1 | 1 | 1 | 0.2 |
| | 2 | 2 | 2 | 1 |
| | 4 | 4 | 4 | 2 |
| | 8 | 8 | 6 | 3 |
| | 12 | 10 | 9 | 4 |
| | 16 | 12 | 12 | 6 |
| | 20 | 16 | 16 | 8 |
| | 24 | 20 | 20 | 10 |
| | 30 | 24 | 24 | 12 |
| | 40 | 30 | 28 | 14 |
| | 73 | 40 | 32 | 16 |
| | - | 50 | 36 | 18 |
| | - | 70 | 40 | 20 |
| | - | 100 | 44 | 24 |
| | - | 130.5 | 48 | 30 |
| | - | 160 | 52 | 35 |
| | - | 200 | 60 | 40 |
| | - | 260 | 70 | 57.2 |
| | - | 320 | 80 | - |
| | - | 400 | 90 | - |
| | - | 500 | 100 | - |
| | - | 700 | 120 | - |
| | - | 830 | 140 | - |
| | - | 1060 | 160 | - |
| | - | 1230 | 180 | - |
| | - | 1340 | 200 | - |
| | - | 1400 | 240 | - |
| | - | 1500 | 280 | - |
| | - | 1600 | 320 | - |
| | - | 1700 | 360 | - |
| | - | 1800 | 400 | - |
| | - | 1900 | 450 | - |
| | - | 2000 | 500 | - |
| | - | 2200 | 600 | - |
| | - | 2500 | 750 | - |
| | - | 2700 | - | - |

of the cold work on the metallography and fractography. One specimen was fatigued axially to produce a short crack and then over-pulled to produce an easily observable plastic zone at the crack tip.

After the fatigue sequence, hardness profiles were developed for each specimen to check for location and degree of strain hardening. Hardness measurements were made on a Leitz microhardness machine using 50 gram weight usually. This created an indentation sized around 25 um.

# CHAPTER IV

# EXPERIMENTAL RESULTS

## Slip Behavior

Both the reversed bending and the axial fatigue samples showed slip markings after the first cycle for all stress levels leading to failure and grain sizes greater than 100 um. Smaller grain sizes developed recognizable slip markings after about 1000 cycles. Slip in bending fatigue occurred throughout the width of the specimen while slip under axial loading was initially confined to the vicinity of the notch root.

The samples which were cold-worked showed intensive monotonic slip between the two notches and slightly less intensity when more than about 2 mm away from the notch center line. Rumpling was clearly evident over the surface of the cold-worked specimens, except where the notches had protected a small amount of material from stress. Also noticed was a small amount of wavy slip where the rumpling was most pronounced.

Under axial loading, slip increased in intensity and number of slip systems as fatigue progressed. Two and three active slip systems in a grain were common. Slip in grains was planar and very fine, without concentrated bands. While

slip band cracks appeared within one grain of the main crack, additional grain boundary or slip band cracking was absent. After failure, wavy slip was found adjacent to the overload zone.

Under reversed bending, slip bands grew in number and intensity. Initiation of slip band cracking was dependent upon stress level and therefore related to the life. Cracking at about 3000 cycles corresponded to Nf=70,000 cycles while cracking at about 200,000 cycles predicted a life well in excess of 3 million cycles. Concerning slip band cracking within a grain, as the first cracks grew, more cracks developed parallel to the first. The cracks would grow to span 90 % of the grain and then stop growing unless they were used in propagating the main crack. This slip band cracking was prevalent across the specimens and within 2 mm of the notch centerline. Occasionally slip bands would link up by cracking along grain boundaries. However, most slip band cracks did not grow past the grain boundary. As shown in figures 6 and 7, later cracking often propagated past or across cracked slip bands without being deflected or noticeably influenced by the presence of the cracks when a grain boundary was available for propagation or when the slip bands angled away from the centerline between the notches.

When axial fatigue was applied to cold-worked specimens, there was little increase in slip markings although slip band cracking was observed within one grain of

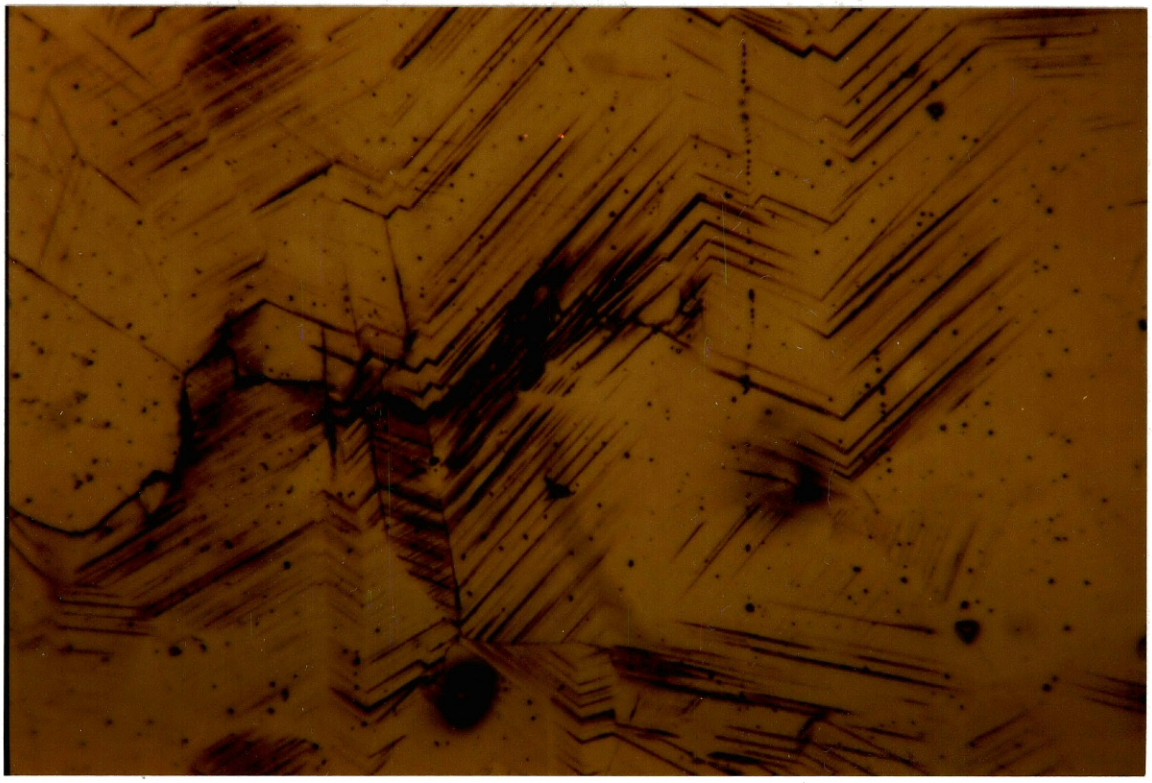

Figure 6. Crack Propagation in Reversed Bending.

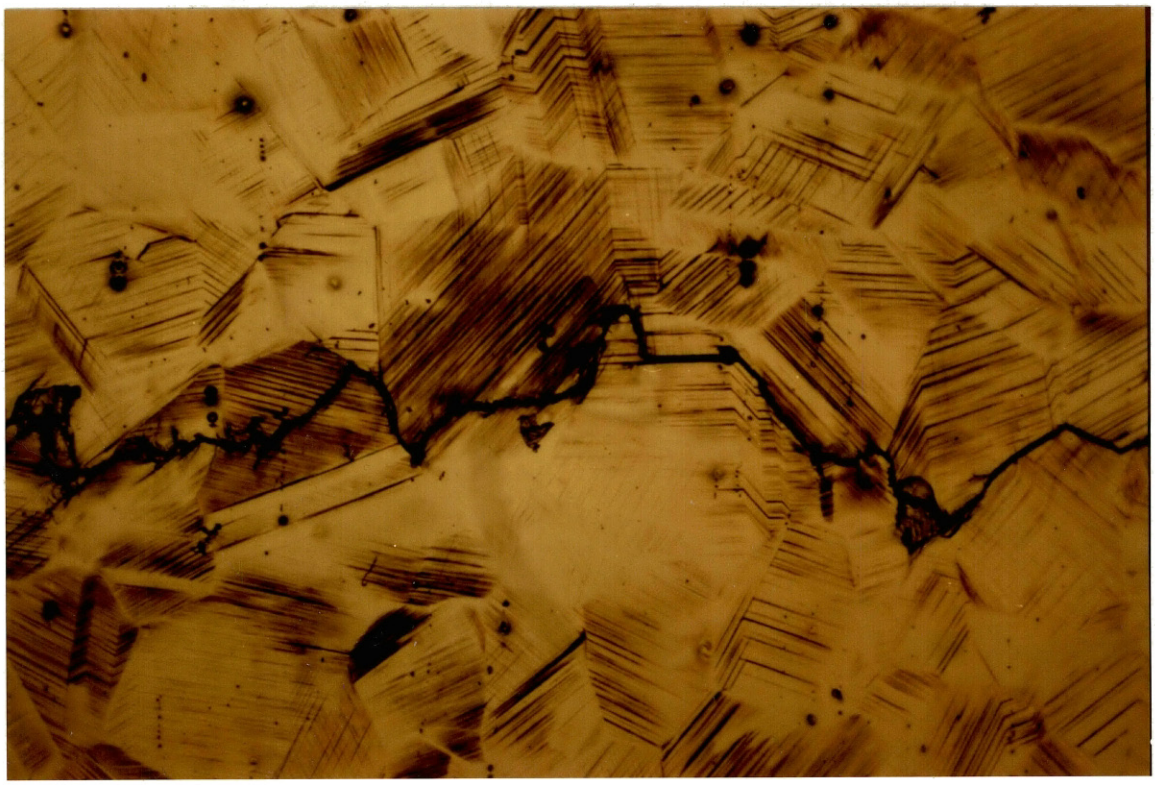

Figure 7. Crack Propagation in Reversed Bending with Cold Work.

the crack. However, greater plastic deformation was imposed upon the material at the crack tip as the crack propagated. The deformation at the crack tip was concentrated along 45 degree shear lines as seen in figure 8.

Reversed bending did not change the slip appearance in cold-worked specimens. Also, plastic deformation was not noticeably increased. Secondary cracking at grain boundaries and slip bands occurred ahead of the main crack as in the other reversed bending specimens. However, the cracks were not quite as numerous as in the non-cold worked specimens.

## Plastic Zone

Surface rumpling was evident in axial fatigue but absent under bending fatigue. Rumpling was slight at the notch root and intensified as the crack progressed across the sample as seen in figure 8. Figure 9 illustrates the lack of deformation in the area adjacent to the notch. Plastic deformation with small grains was more confined to the area of the crack than in the large grain case.

## Crack Initiation

Cracks initiated at about 5% of the expected life for reversed bending and about 30% of the life for axial fatigue, independent of grain size and stress magnitude. Under bending fatigue slip bands often cracked in several

Figure 8. Surface Rumpling Under Axial Fatigue.

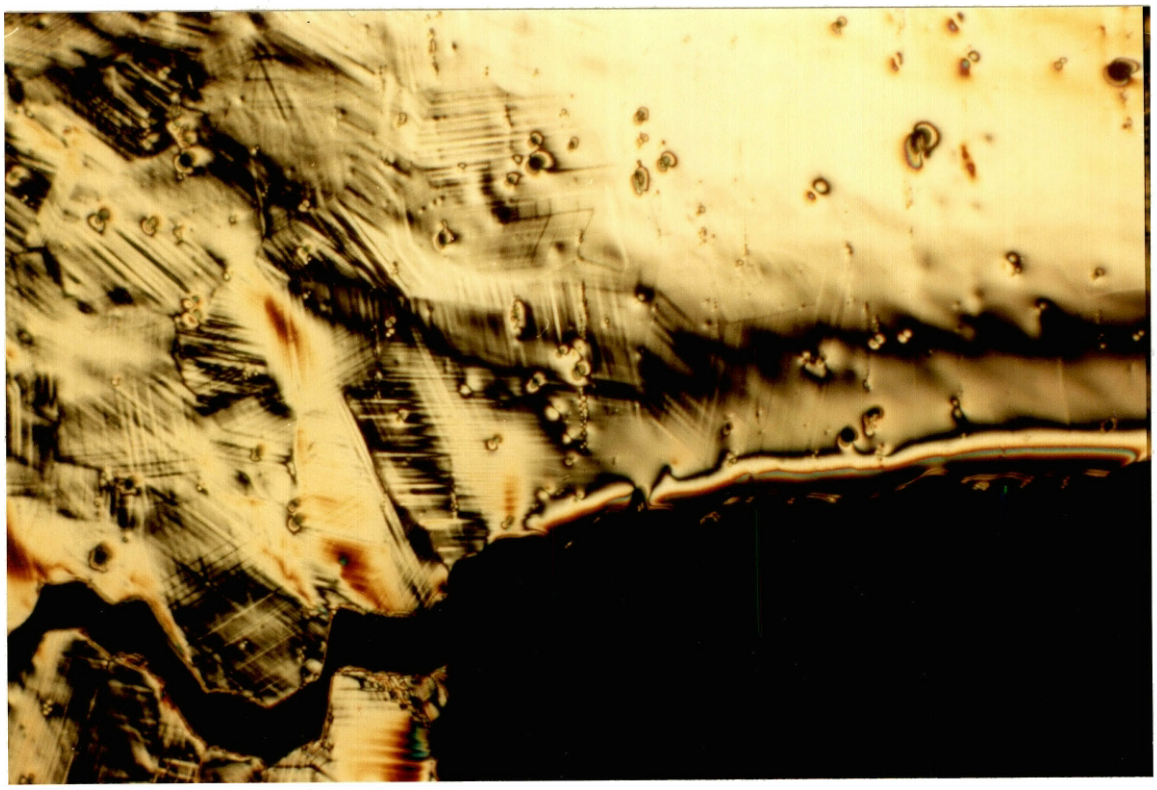

Figure 9. Plastic Deformation at Notch.

grains next to the notch root. However, the main crack only started along slip bands or twins which reached the notch. Initial propagation was very rapid but slowed as the crack progressed. Grain boundaries sometimes cracked ahead of the crack tip, providing a boost to the propagation rate when reached and transition to IG cracking.

Slip band cracking was not observed in axial fatigue until after the crack had initiated, and then only immediately adjacent to the crack. As in bending, initiation was crystallographic and there was an initial burst of speed which decreased over the first 1500 um and then increased until failure. Cracks were TG until they met a favorably aligned grain boundary, thence became predominately IG.

## Crack Growth

Cracking produced by axial fatigue tended to be along grain boundaries and twins and usually followed a 45 degree path microscopically although macroscopic fracture appeared flat. Sometimes the crack would split with each branch angled 45-60 degrees from the direction of propagation as seen in figure 10. The crack would then continue along one of the branches or occasionally the branches would merge to continue the crack. Although the specimens were double notched and aligned in the grips, cracks tended to grow from one notch in axial fatigue until near failure; when a crack

Figure 10. Crack Branching.

would often initiate from the second notch. This is in contrast to bending fatigue where cracks grew relatively evenly from both notches.

Crack growth for axial fatigue is illustrated by figures 11, 12, and 13 which compare a vs N, da/dN vs a, and da/dN vs dK respectively. In figure 11, for both coarse and fine grain sizes, the crack length wavers in its initial growth and then grows exponentially to failure. Note that while the fine grain crack initiated about 20,000 cycles before the coarse grain, the final failure with the fine grain occurred 100,000 cycles sooner. This is related to the increased amount of IG cracking which occurred with a fine grain size. Figure 12 shows that while initial crack growth rates waver, after about 1300 um the cracking in the fine grain specimen propagates at an increasingly faster rate than the coarse grain case. As seen in figure 13, cracking in Monel follows the Paris equation with slope of about 2.5 which agrees with Richards (31).

Secondary cracking along slip lines and grain boundaries was only observed with bending fatigue. This secondary cracking eventually frustrated attempts to gather relevant crack growth data. When the main crack unexpectedly grew slowly or not at all, the cause was often secondary crack growth which relieved the strain on the main crack. Such cracking occurred regardless of grain size, and increasingly during the life of the specimens; thereby

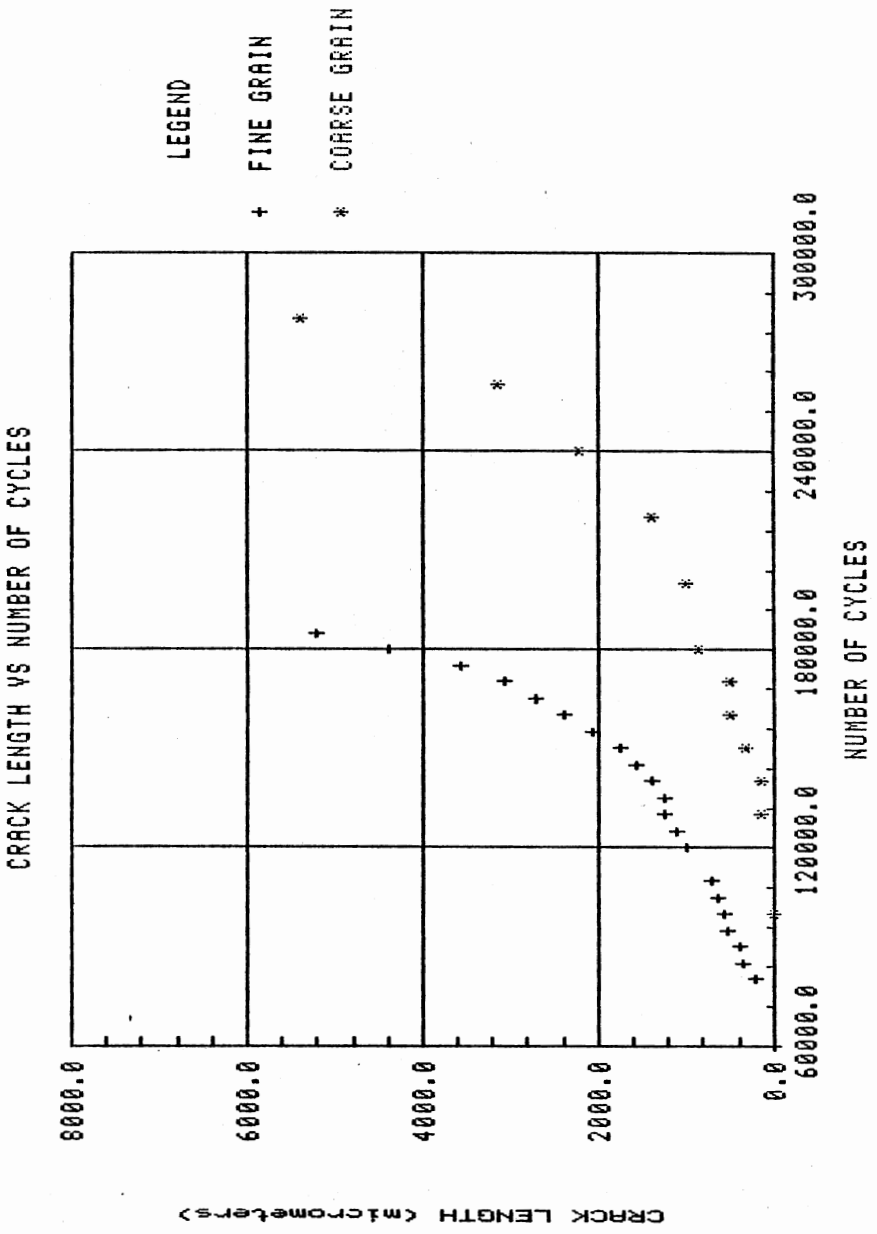


Figure 11. Crack Length vs Number of Cycles.

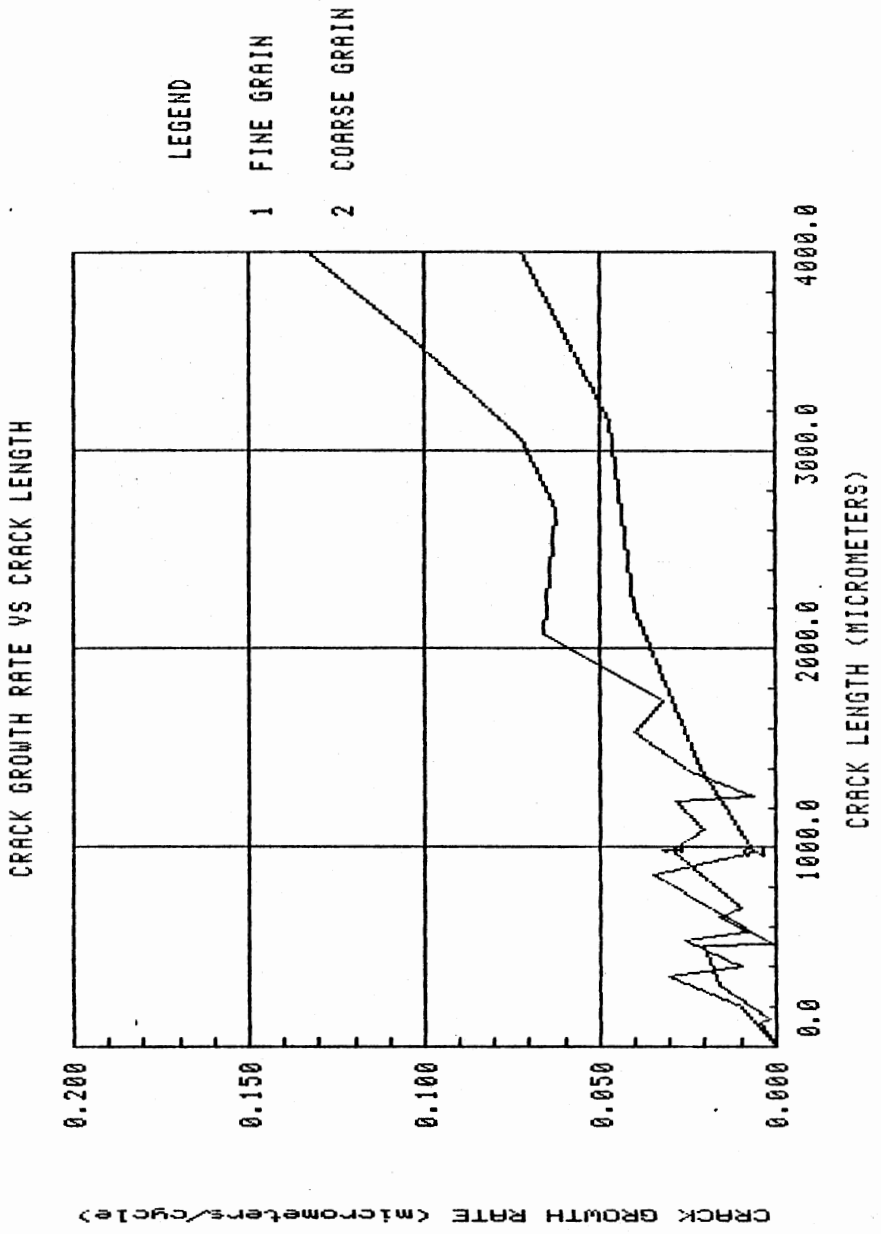


Figure 12. Crack Growth Rate vs Crack Length.

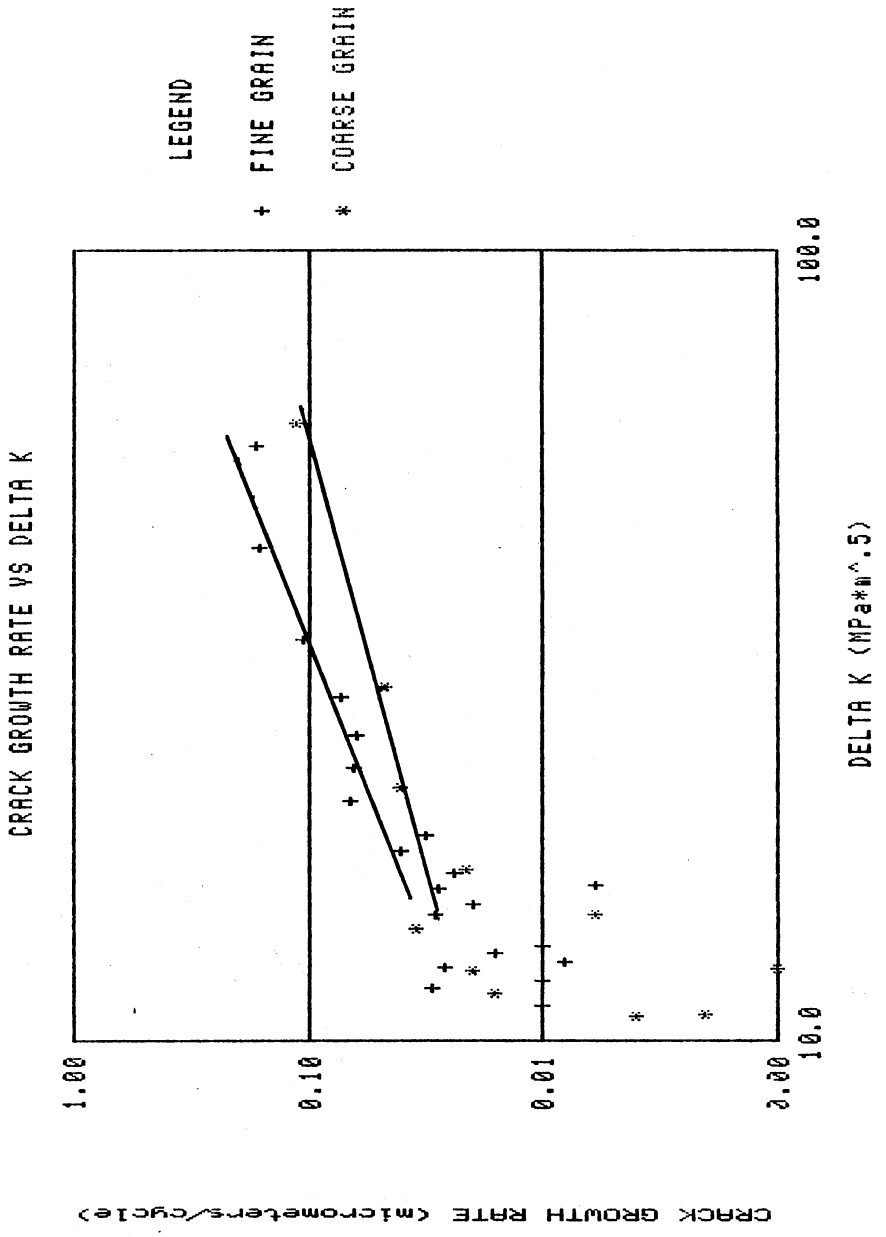


Figure 13. Crack Growth Rate vs Stress Intensity Range.

decreasing the rate of crack propagation on the monitored cracks. A cold-worked specimen, subsequently fatigued in reversed bending, showed secondary cracking although to a lesser extent.

Although cracks in reversed bending occasionally propagated along cracked slip bands, the preferred route was along grain boundaries and twin boundaries. A main feature of the cracking in both axial and bending fatigue was its zigzag nature as show in figure 14. Cracking tended to follow a path 45 degrees from the load axis. On many occasions the crack would start to fork and then rejoin to create a single path again as seen in figure 15.

Typical bending fatigue crack growth is illustrated in figures 16, 17 and 18 for specimens with lives of greater than 2.5 million, about 1 million, and 73,000 cycles respectively. Note that as in axial fatigue, the crack growth was irregular for the first 3-4 grains. After the crack had penetrated 4 grains, the growth rate decreased as secondary cracking became prevalent.

## Fatigue Hardening

After axial fatigue, the hardness profiles correlated with the observed plastic zone around the cracks for both coarse and fine grain sizes. As the crack grew, hardening next to the crack increased and the hardened zone increased in size. The result was similar for both fine and coarse

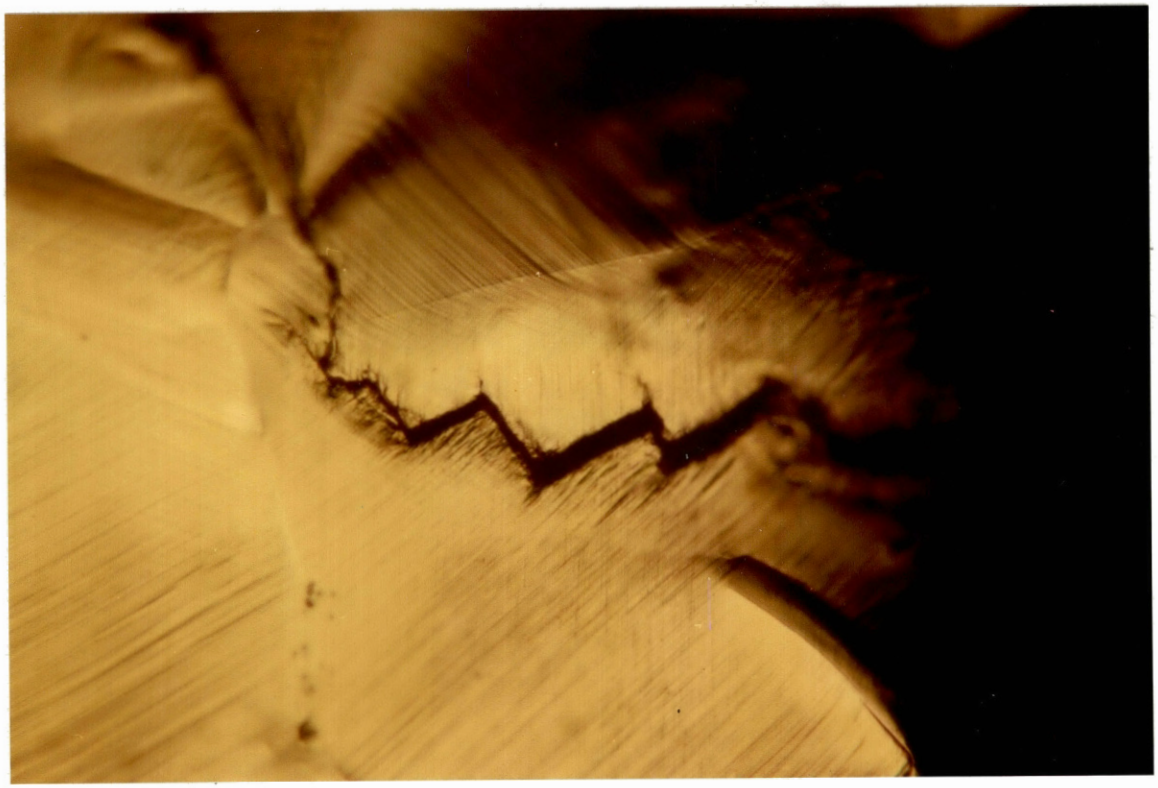

Figure 14. Cracking Under Axial Loading.

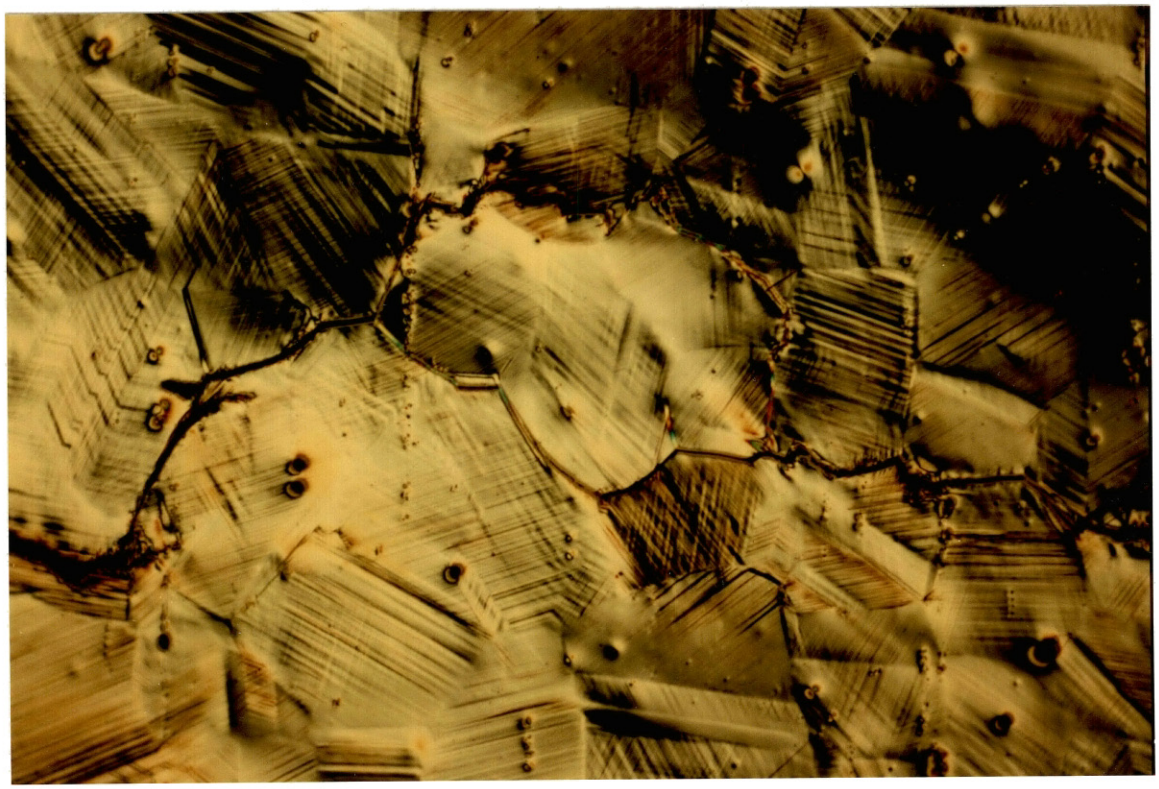

Figure 15. Cracking Under Reversed Bending.

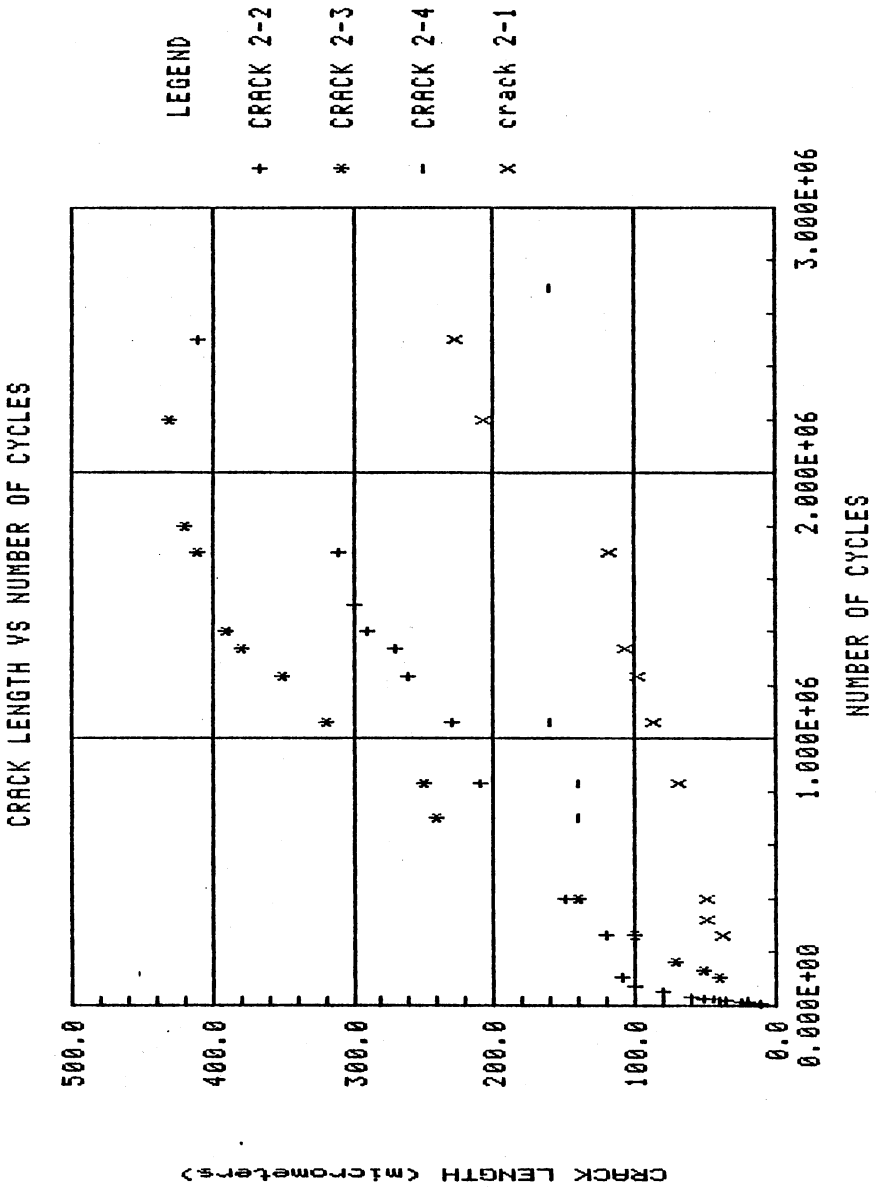


Figure 16. Crack Length vs Cycles for Reversed Bending, Life Greater than 2.5 Million Cycles.

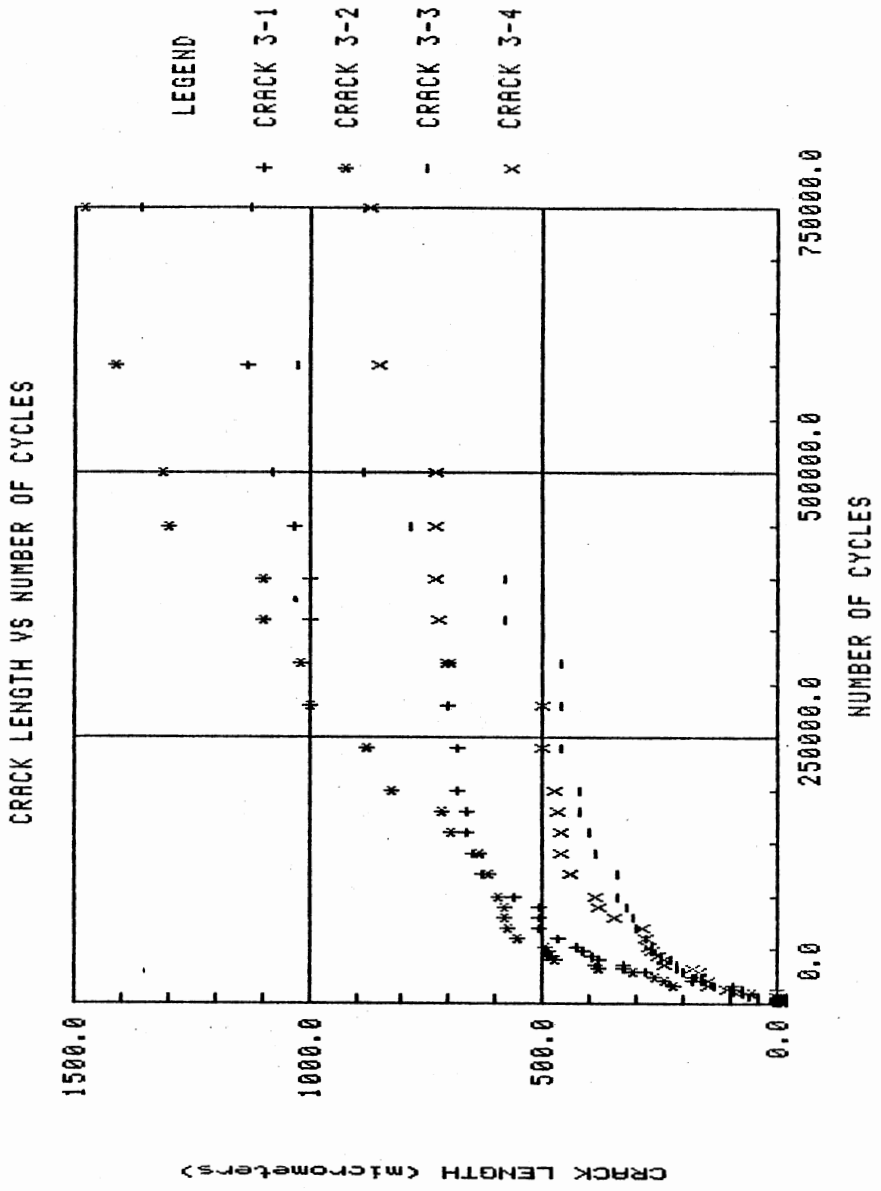


Figure 17. Crack Length vs Cycles for Reversed Bending, Life of About 1 Million Cycles.

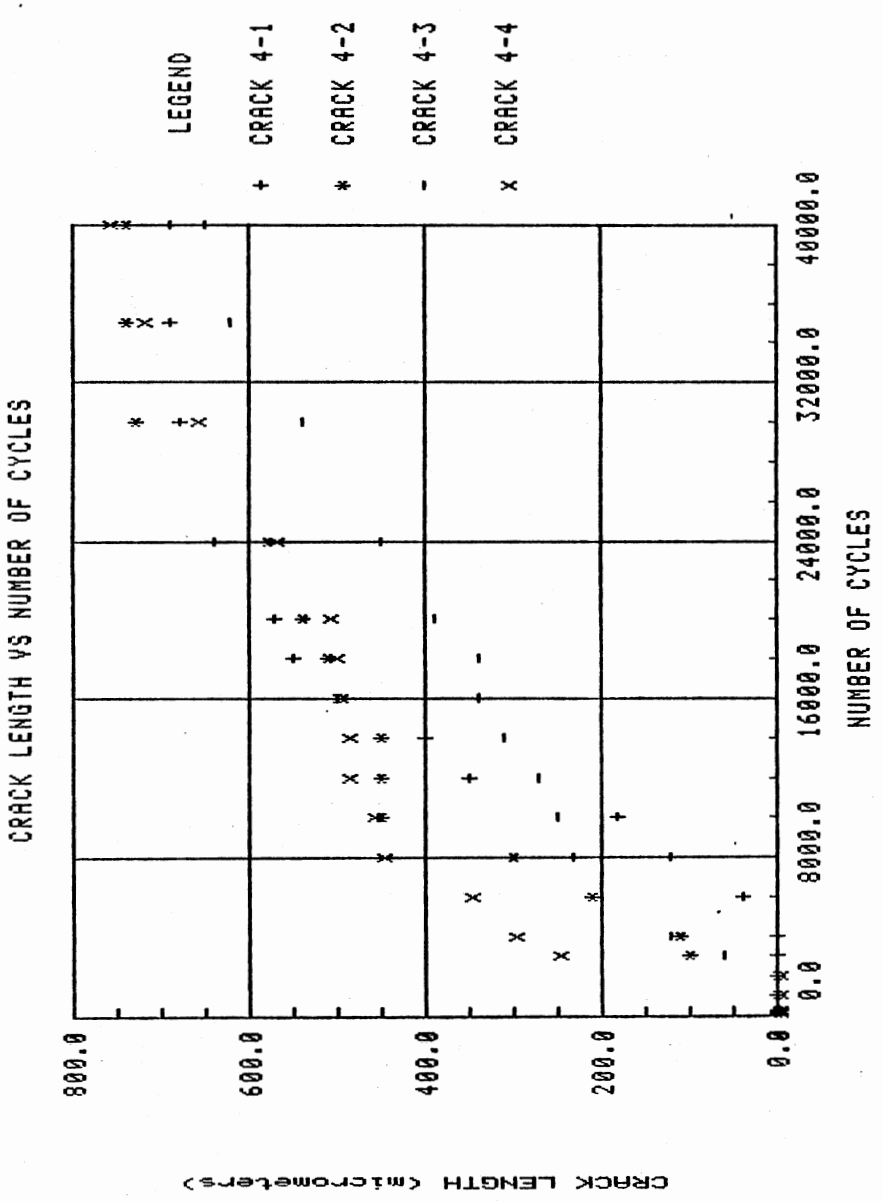


Figure 18. Crack Length vs Cycles for Reversed Bending, Life Equal to 73,000 Cycles.

grain sizes as seen in figures 19 and 20.

With axial fatigue and a 25 um grain size, hardness values behind the notches were about 130 HV increasing to 140 at the notch root. Then, the hardness along the line of the crack gradually increased to about 200 HV and the width of the hardness zone increased to about 4 mm from the crack. As the other notch was reached, the hardness fell abruptly. Coarse grains yielded a similar profile, hardening from 130 HV beside the notch to 160 at the notch root. The hardness increased along the line of the crack to about 200 HV and the hardness zone extended to about 4 mm from the crack. A hardness profile on an unbroken specimen showed similar features, with hardening occurring ahead of the crack tip as seen in figure 21. Prior cold-work gave higher hardness values at notch root of about 170-180 HV, but otherwise no difference.

Bending fatigue results on fine grain size specimens were consistent with the report by Henderson (27), with 25-30 HV of hardening occurring at the crack, dropping quickly to define a hardening zone extending 1 mm from the crack line. Although the crack was propagating from the notches, there was no difference in hardening along the crack line.

The coarse grain specimens in bending fatigue showed a larger hardening zone, extending 2 mm from the crack. As with the fine grain size, about 30 points of hardening was found along the crack line.

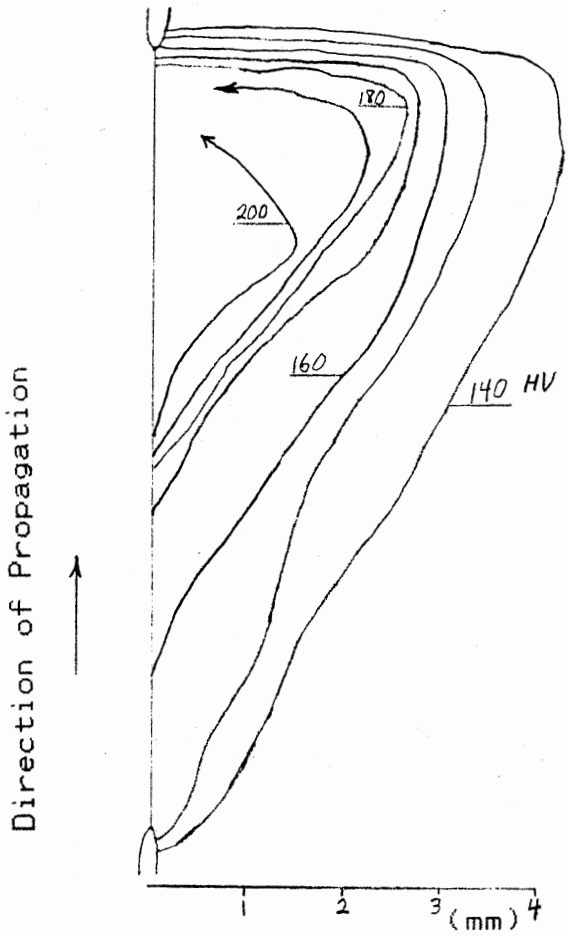


Figure 19. Axial Hardness Profile for Coarse Grains.

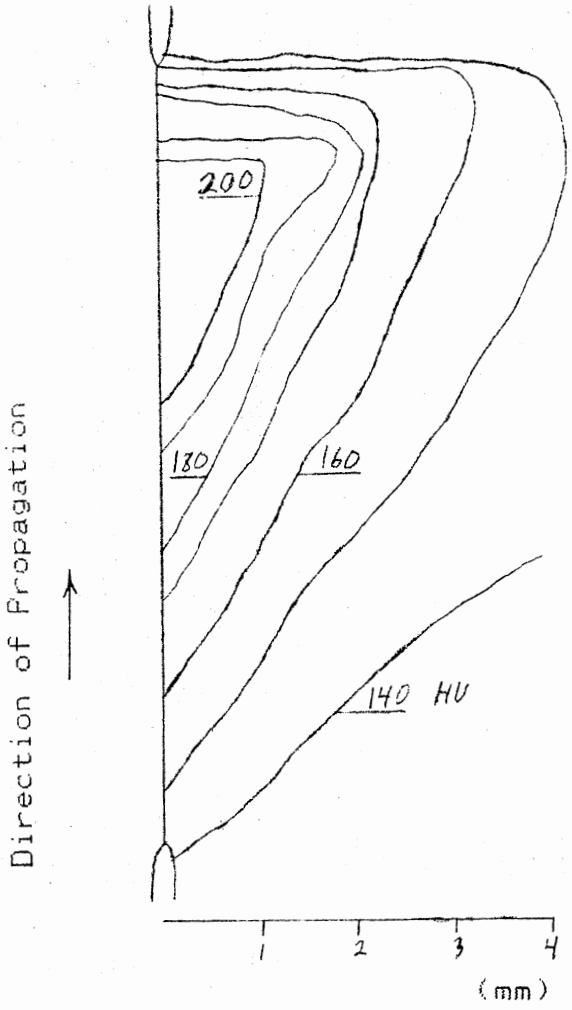


Figure 20. Axial Hardness Profile for Fine Grains.

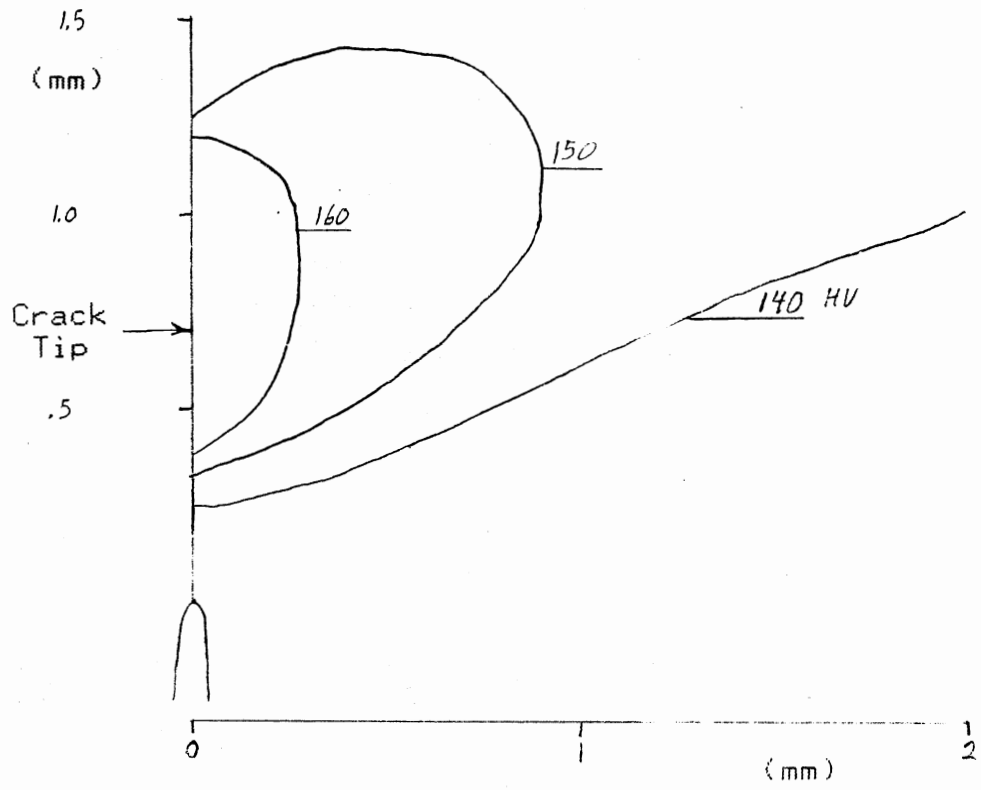


Figure 21. Axial Hardness Profile for an Unbroken Specimen.

## Cracking Mode

The fracture surface for bending fatigue was a mix of IG and TG fracture. A parting line ran from one notch to the other in the center of the sample, occasionally interrupted by part of the facet of a grain.

Axial fatigue produced a fracture surface which showed four stages of fracture regardless of cold-work or specimen life. Starting at the notch was a region of predominately transgranular fracture about one grain deep. The mode then changed to predominantly IG fracture with the proportion of IG fracture decreasing with increasing grain size. IG growth dominated for the next 3 mm. In coarse grained specimens, IG cracking made a transition to TG cracking over about .5 mm. Cracking continued by TG propagation and then TG with fatigue striations. Final failure was by microvoid coalescence. While the same progression was followed by fine grained specimens, the transitions from one mode to the next were more distinct. Also noted, the fracture surface changed from flat to a slight slant during the transition to TG propagation.

The percent of IG fracture in both bending fatigue and the first stage of axial fatigue was dependent upon the grain size. Small grain sizes showed nearly 100% IG fracture while increasing the grain size to 500 um would decrease, but not eliminate, IG cracking as seen in figure 22.

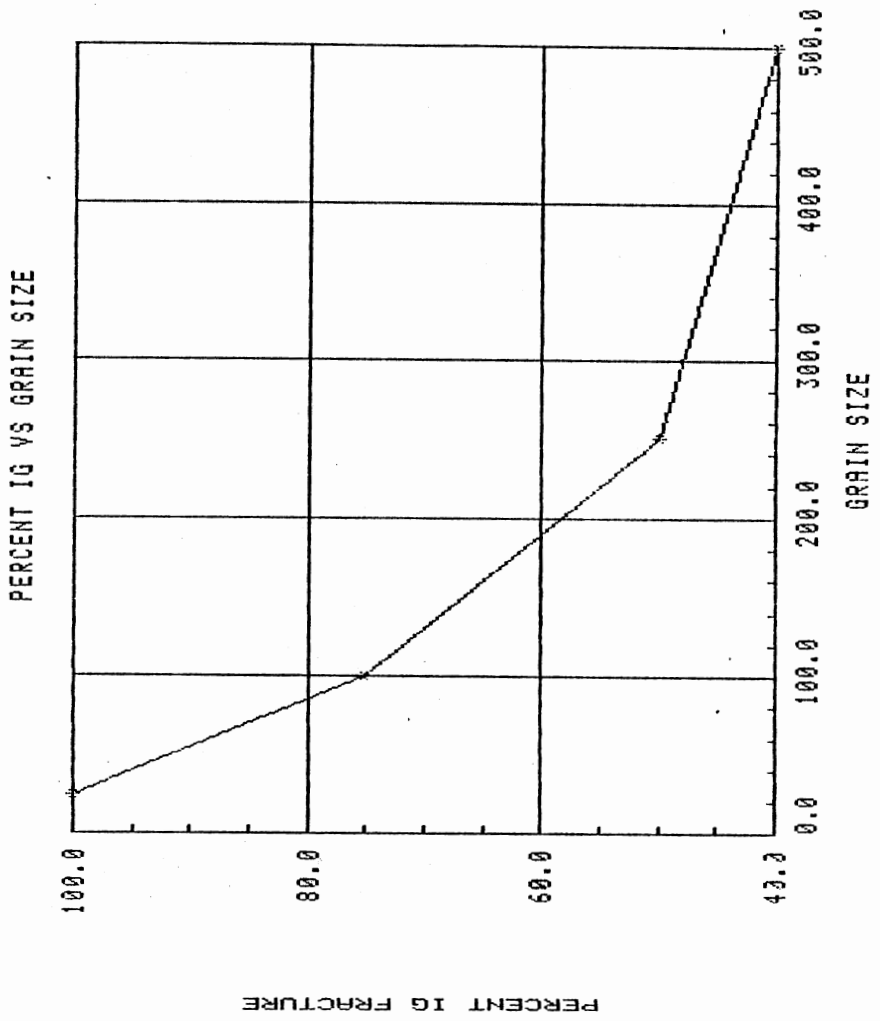


Figure 22. Percentage IG Fracture vs Grain Size.

# CHAPTER IV

# DISCUSSION

This investigation has focused upon the prevalence of IG cracking in a Ni-Cu alloy. Of all the nickel base alloys, the Monel alloys are the only ones which demonstrate IG fatigue cracking without an obvious cause.

A coarse grain size decreased the degree of IG fracture but did not eliminate it. This is similar to the results of Fredell (24), who found HE decreased by increased grain size and LME by mercury decreased by grain sizes above 250 um. However, IG cracking decreased with crack propagation under axial fatigue, thus increased stress intensity range led to TG propagation. Fredell (24) found similar results in that increasing strain rate decreased embrittlement. Although plastic deformation increased with increasing dK, the previously cold-worked specimens still showed IG cracking. However, it is noted that dK must be high enough to produce surface rumpling for transition from IG to TG.

Often, IG cracking is associated with grain boundary segregation of elements such as with sulfur. This has been investigated in previous studies for many nickel alloys and nickel itself (4,17,33). Costas (6) and Funkenbusch, Heldt, and Stein (9) demonstrated a lessening of LME by mercury

when phosphorus was segregated at grain boundaries. However, segregation is not thought to play a part in the present study as the IG behavior was not related to heat treatment. The study by Fredell (24) involved slow cooling after different heat treatment temperatures and times to obtain different grain sizes in the alloy. Henderson (27), who quenched and aged his samples, found no difference in cracking behavior for SHT, OVA, or OPA specimens. The present study used different times at high temperature followed by a water quench to obtain a range of grain sizes. This was followed by different times at room temperature before testing, yet no inconsistencies concerning IG cracking were found and in no situation was IG cracking eliminated. Sulfur is not thought to be a factor as Traylor and Price (32) found somewhat less HE and LME with the high sulfur grade, Monel 405, than with Monel 400.

Consider crack growth in bending as compared with nickel in bending by Ho (11). Despite the prevalence of IG cracking, crack initiation in Monel was largely TG as is nickel. However, crack initiation in Monel meant the life was more nearly over than with nickel. After initiation occurred in nickel, 99% of the life remained. With Monel in bending, crack initiation meant 95% of the life remained. Apparently crack propagation occurs more readily in Monel. Irregular early growth was a feature for both materials and for all grain sizes in Monel. Ho (11) used a 400-500 um grain size to facilitate observations and comparable grain

size in the present study does mimic the initial irregular crack growth behavior of nickel. However, the three-grain effect, as mentioned by Ho (11), was not seen in the fine grain size as seen in figure 12. Irregular growth in fine and coarse grains lasted for about the same distance.

With bending in both nickel and Monel, slip band cracking was prevalent. Branching and secondary cracking were more severe in low cycle bending than high and appeared insensitive to grain size. This secondary cracking relieved stress on the main crack which caused a decrease in the propagation rate, thus the decreasing slope on the crack growth curves. While these curves do describe the growth of the main crack, they do not reflect the overall damage which is accumulating in the specimen. A casual observer might assume the damage accumulation rate was lessening, therefore attempting to use these curves for crack growth behavior in a design situation would be foolhardy.

Initiation dominated the life of axial specimens. Once a crack was recognized under axial fatigue, the life was about 1/3 over rather than 5% over as in the bending case. This difference may be caused by slower initiation, faster propagation, or a combination of the two.

Examine Neumann's (20) model for initiation for reversed bending and axial fatigue. Under reversed bending the material was cycled from tension into compression. This is Neumann's driving force to create intrusions and extrusions and thereby initiate cracking. The widespread

slip band cracking between the notches in bending lends support to this model.

If Neumann's (20) model is applied to the axial case, macroscopically there should be no extrusions or intrusions since the fatigue was in tension-tension. However, microscopically the material at the center of the notch was put into compression in the low load part of the cycle due to elastic recovery of the material on either side. This provided a small area at the crack tip which had a compression-tension cycle which could initiate cracking. Such a zone would be small which agrees with the observed absence of widespread cracking. Compression would be greatest at the crack tip, therefore cracking would be more likely at the crack tip which corresponds with the observed absence of cracking ahead of the crack in axial fatigue.

A zone of heavy plastic deformation was observed to emanate at about 45 degree angles from the crack tip. This corresponds to the angle of greatest shear which has been described by Brown (2).

The hardening correlated with observed plastic deformation. For example, as the crack progressed under axial fatigue, the plastic deformation and the hardening both increased. This makes sense, increased plastic deformation at ambient temperatures corresponds to an increase in hardness in materials with a work hardening capability. The increase seen under axial fatigue was due to an increase in dK as the crack grew. The hardening in

front of the crack during axial fatigue closely matches the expected plastic zone as described by Hertzberg (10).

Cracks in both bending and axial loading tended to propagate in an zigzag fashion and branched quite often. This is in agreement with both the maximum shear described by Brown (2) and the stage II propagation described by Neumann (20).

Bending fatigue produced a homogeneous mixture of IG and TG fracture with a lower percentage of IG fracture associated with increased grain size. The same mixture of IG and TG fracture was seen in the first stage of axial fatigue crack growth. A later transformation eliminated the IG cracking entirely. It is reasoned that low stress intensity, such as under bending fatigue or the first section of axial fatigue, allows IG propagation to occur by unknown mechanism. However, higher stress intensity either disables or negates this mechanism so that a plastic blunting mode as described by Laird (14) may dominate.

With fine grain size, figure 23 ,the transformation from IG to TG cracking was better defined. Notably, the crack propagation rate was higher with fine grain size, presumably due to the nearly pure IG zone.

Of interest is the slip behavior. Slip was seen early in the life of all specimens. Bending fatigue commonly exhibited secondary and ternary slip systems and all slip was planar as is seen with low stacking fault materials. Axial fatigue produced the same slip initially but wavy slip

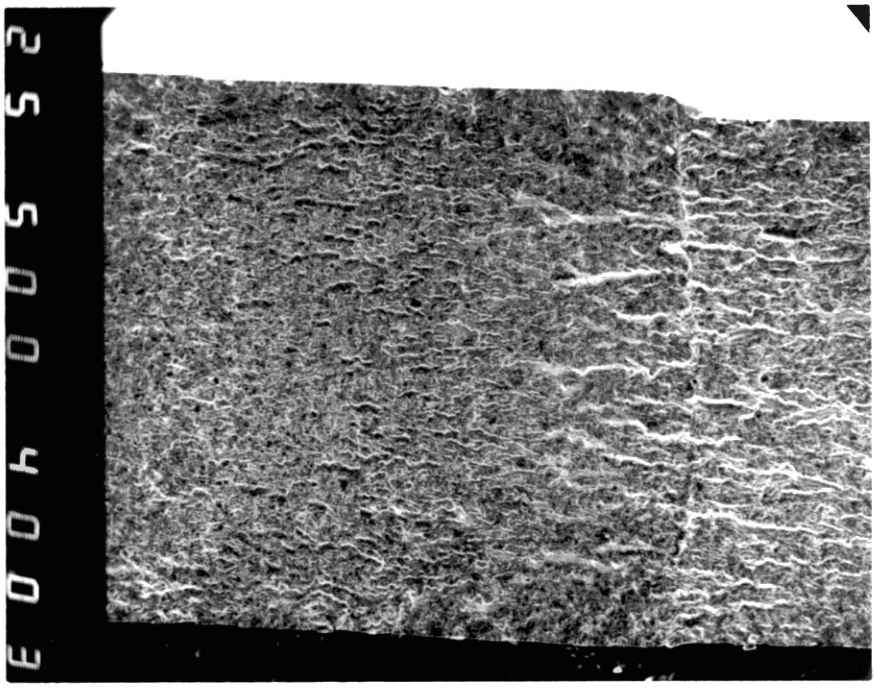


Figure 23. Fine Grain Axial Fatigue Fracture Surface.

became visible in the last stages of axial fatigue as it did during severe cold-working. Due to its requirement of cross-slip, wavy slip is characteristic of high SFE materials. However, a material with medium SFE may exhibit both planar and wavy slip (10). Thus, as the stress increased, partial dislocations were united and cross-slip was activated.

As in Henderson (27), inclusions were found not to matter in this study. Cracking did not initiate at inclusions and propagation cracks did not veer towards or away from inclusions.

Considering the ready IG cracking in air and the crack initiation behavior of Monel, caution is advised when this alloy is used in fatigue. Under axial loading, a significant portion of the life is used for crack initiation. An active environment, common in Monel applications, could decrease an already short crack life.

# CHAPTER VI

## CONCLUSIONS

1. Fatigue fracture of Monel in air is partly IG. This occurs for different grain sizes, heat treatments, cooling rates, and whether the test mode is axial or bending. The proportion of IG fracture decreased with increased grain size or dK. With a fine grain size of 25 um, initial cracking was almost entirely IG.

2. While crack initiation was usually along slip bands, initiation sometimes occurred along grain boundaries.

3. In both axial and bending fatigue, crack growth was irregular for about the first millimeter. Later growth under axial loading could be predicted by LEFM despite continued IG cracking.

4. In bending fatigue, displacement control, 95% of the life remained after cracks were initiated and many secondary cracks later formed ahead of and next to the crack tip. In axial fatigue, load control, about 70% of the life was left after cracking was detected.

5. The plastic deformation zone at the crack tip and near the notch root could be observed initially with Nomarski contrast interference microscopy, and later with white light microscopy. The intensity of plastic deformation coincided with degree of hardening. In axial fatigue, increased stress intensity yielded increased plastic deformation and increased hardening.

6. A coarse grain size facilitated observation of slip character which was largely planar. Cross slip was observed in the overload zone.

7. Fatigue properties of Monel are poor as fatigue failure occurs at stresses well below the yield stress. The propensity for IG propagation under EAC and in air indicates caution is merited when Monel is used in a load bearing application.

## A SELECTED BIBLIOGRAPHY


1. American Society For Metals, Metals Handbook, 9th edn, Vol. 3, Metals Park, Ohio, 1980, pp. 128-170.

2. Brown, M. W., "Interfaces Between Short, Long, and Non-Propagating Cracks" The Behaviour of Short Fatigue Cracks, Paston Press, Norwich, 1986, pp. 423-439.

3. Budinski K. J., Engineering Materials Properties and Selection, 2nd edn. Reston, Virginia, 1983.

4. Chaung, H., J. B. Lumsden, and R. W. Staehle, "Effect of Segregated Sulfur on the Stress Corrosion Susceptibility of Nickel." Metallurgical Transactions, Vol. 10A, December 1979, pp. 1853-1857.

5. Copson, H. R. and C. F. Cheng, "Stress Corrosion Cracking of Monel in Hydrofluoric Acid." Corrosion, Vol. 12, No. 12, 1956, pp. 71-77.

6. Costas L. P., "Effect of Phosphorus on the Embrittlement of Copper-Nickel Alloys by Mercury." Corrosion, Vol. 31, No. 3, 1975, pp. 91-96.

7. Efird, K. D., "Failure of Monel Ni-Cu-Al Alloy K-500 Bolts in Seawater." Materials Performance, Vol. 24, April 1985, pp. 37-40.

8. Everhart, L. G., "Stress Corrosion Cracking in Monel 400." (Unpub. M.S. thesis, Oklahoma State University, May 1989.)

9. Funkenbusch, A. W., L. A. Heldt, and D. F. Stein, "The Influence of Grain Boundary Phosphorus Concentration on Liquid Metal and Hydrogen Embrittlement of Monel 400." Metallurgical Transactions, Vol. 13A, April 1982, pp. 611-618.

10. Hertzberg R. W., Deformation and Fracture Mechanics of Engineering Materials, John Wiley & Sons, New York, 1976.

11. Ho, Yiao-Teng, "The Fatigue Crack Behavior of Notched Nickel." (Unpub. M.S. report, Oklahoma State University, May 1989.)

12. Huntington Alloy Products Division of the International Nickel Company, Inc., Engineering Properties of Monel Alloy K-500, Tech. Bull. T-9, Huntington, WV, 1965.

13. Kotval, P. S., "The Microstructure of Superalloys." Metallography, Vol. 1, 1969, pp. 251-285.

14. Laird, C., "The Influence of Metallurgical Structure on the Mechanisms of Fatigue Crack Propagation." Fatigue Crack Propagation, ASTM STP 415, American Society For Testing and Materials, 1967, p. 131.

15. Lassila, D. H., and H. K. Birnbaum, "The Effect of Diffusive Hydrogen Segregation on Fracture of Polycrystalline Nickel." ACTA Metallurgica, Vol. 34, 1986, pp. 1237-1243.

16. Mellor, B. G., K. Tabeshfar, and G. A. Chadwick, "Failure by Liquid Metal Embrittlement in Monel 400." The Metallurgist and Materials Technologist, September 1982, pp.385-386.

17. Messmer, R. P., and C. L. Briant, "The Role of Chemical Bonding in Grain Boundary Embrittlement." ACTA Metallurgica, Vol. 30, 1982, pp. 457-467.

18. Miller, K. J., and de los Rios E. R. Eds., The Behaviour of Short Fatigue Cracks, Paston Press, Norwich, 1986.

19. Morris, W. L., J. D. Frandsen, and H. L. Marcus, "Environmentally Induced Transitions in Fatigue Fracture Mode." Fractography-Microscopic Cracking Processes, ASTM STP 600, American Society for Testing and Materials, 1976, pp. 49-61.

20. Neumann, P., H. Fuhlrott, and H. Vehoff, "Experiments Concerning Brittle, Ductile, and Environmentally Controlled Fatigue Crack Growth." Fatigue Mechanisms, ASTM STP 675, American Society for Testing and Materials, 1979, pp. 371-395.

21. Parikh, N. M., "Embrittlement of Solid Solution Alloys of Nickel and Palladium by Molten Lithium, Environmental Assisted Cracking, Transactions of ASME, 1962, pp. 563-579.

22. Paris, P. C., Fatigue--An Interdisciplinary Approach, Proceedings 10th Sagamore Conference, Syracuse University Press, Syracuse N. Y., 1964, p.107.

23. Price C. E., "The progression of bending fatigue in Nickel." Fatigue Fract. Engng Mater. Struct., Vol. 11, 1988, pp. 483-491.

24. Price, C. E., and R. S. Fredell, "A Comparative Study of the Embrittlement of Monel 400 at Room Temperature by Hydrogen and Mercury.", Metallurgical Transactions, Vol. 17A, May 1986, pp. 889-898.

25. Price, C. E., and J. K. Good, "The Fatigue Behavior of Nickel, Monel, and selected superalloys tested in Liquid-Mercury and Air; a Comparison." American Society of Mechanical Engineers Transactions, Vol. 106, 1984, pp. 178-183.

26. Price, C. E., and J. K. Good, "The Tensile Fracture Characteristics of Nickel, Monel and Selected Superalloys Broken in Liquid Mercury." American Society of Mechanical Engineers Transactions, Vol. 106, 1984, pp. 184-190.

27. Price, C. E., and G. W. Henderson, "The progression of bending fatigue in Monel K500." Fatigue Fract. Engng Mater. Struct.,Vol. 11, 1988, pp. 493-500.

28. Price, C. E., and N. R. Houghton, "The progression of bending fatigue in Inconel 625." Fatigue Fract. Engng Mater. Struct., Vol. 11, 1988, pp. 501-508.

29. Price, C. E., and J. A. Morris, "The Comparative Embrittlement of Example Nickel Alloys by Hydrogen and Mercury." Journal of Materials for Energy Systems, American Society for Metals, Vol. 7, No. 3, Dec. 1985, pp. 246-255.

30. Purushothaman, S., R. J. Richards, J. K., Tien and J. D. Frandsen, "Kinetics of Environmental Fatigue Crack Growth in Nickel-Copper Alloy: Part I. In Vacuum and Oxygen." Metallurgical Transactions, Vol. 9A, August 1978, pp. 1101-1105.

31. Richards, R. J., S. Purushothaman, J. K. Tien, J. D. Frandsen, and O. Buck, "Kinetics of Environmental Fatigue Crack Growth in Nickel-Copper Alloy: Part II. In Hydrogen." Metallurgical Transactions, Vol. 9A, August 1978, pp. 1101-1105.

32. Traylor, L. B., and C. E. Price, "A Comparison of Hydrogen and Mercury Embrittlement in Monel at Room Temperature." Journal of Engineering Materials and Technology, Vol. 108, June 1986, pp. 31-36.

33. Westbrook, J. H. and S. Floreen, "Kinetics of Sulfur Segregation at Grain Boundaries and the Mechanical Properties of Nickel." Canadian Metallurgical Quarterly, Vol. 13, No. 1, 1974, pp. 181-186.

VITA

GEORGE O. WILSON

Candidate for the Degree of

Master of Science

Thesis: A STUDY OF FATIGUE CRACK INITIATION AND SHORT CRACK GROWTH IN A MONEL ALLOY

Major Field: Mechanical Engineering

Biographical:

Personal Data: Born in Oklahoma City, Oklahoma, December 15, 1958, the son of James W. and Mary E. Wilson.

Education: Graduated from Field Kindley Memorial High School, Coffeyville, Kansas, in May 1977; received Bachelor of Science Degree in Mechanical Engineering from Oklahoma State University in December 1987; completed requirements for the Master of Science degree at Oklahoma State University in July, 1989.

Professional Experience: Teaching Assistant, Department of Mechanical Engineering, Oklahoma State University, August, 1988, to May, 1989.